## Runaway migration and the formation of hot Jupiters

F. S. Masset<sup>1</sup>

Service d'Astrophysique, CE-Saclay, 91191 Gif/Yvette Cedex, France

fmasset@cea.fr

and

J. C. B. Papaloizou

Astronomy Unit, School of Mathematical Sciences, Queen Mary University of London, Mile End Road, London E1 4NS, United Kingdom

J.C.B.Papaloizou@qmul.ac.uk

## **ABSTRACT**

We evaluate the coorbital corotation torque on a migrating protoplanet. The coorbital torque is assumed to come from orbit crossing fluid elements which exchange angular momentum with the planet when they execute a U-turn at the end of horseshoe streamlines. When the planet migrates inward, the fluid elements of the inner disk undergo one such exchange as they pass to the outer disk. The angular momentum they gain is removed from the planet, and this corresponds to a negative contribution to the corotation torque, which scales with the drift rate. In addition, the material trapped in the coorbital region drifts radially with the planet giving a positive contribution to the corotation torque, which also scales with the drift rate. These two contributions do not cancel out if the coorbital region is depleted, in which case there is a net corotation torque which scales with the drift rate and the mass deficit in the coorbital region, and which has same sign as the drift rate. This leads to a positive feedback on the migrating planet. In particular, if the coorbital mass deficit is larger than the planet mass, the migration rate undergoes a runaway which can vary the protoplanet semi-major axis by 50 % over a few tens of orbits. This can happen only if the planet mass is sufficient to create a dip or gap in its surrounding region, and if the surrounding disk mass is larger than the planet

<sup>&</sup>lt;sup>1</sup>Send offprint requests to F. S. Masset: fmasset@cea.fr

mass. This typically corresponds to planet masses in the sub-Saturnian to Jovian mass range embedded in massive protoplanetary disks. Runaway migration is a good candidate to account for the orbital characteristics of close orbiting giant planets, most of which have sub-Jovian masses. These are known to cluster at short periods whereas planets of greater than two Jovian masses are rare at short periods indicating a different type of migration process operated for the two classes of object. Further, we show that in the runaway regime, migration can be directed outwards, which makes this regime potentially rich in a variety of important effects in shaping a planetary system during the last stages of its formation.

Subject headings: Planetary systems: formation — planetary systems: protoplanetary disks — Accretion, accretion disks — Methods: numerical — Hydrodynamics

#### 1. Introduction

The study of the tidally induced migration of protoplanets embedded in protoplanetary disks has received renewed attention in the last few years following the discovery of extrasolar giant planets (hereafter EGPs). It is in particular the best candidate to explain the short period EGPs (the so-called hot Jupiters) which are likely to have begun to form further out in the disk and migrated radially inwards.

When the planet mass is small (i.e. when its Hill radius is much smaller than the disk thickness), the migration rate can be evaluated using linear analysis, and is shown to be proportional to the planet mass, to the disk surface density, and inversely proportional to the square of the disk aspect ratio (Ward 1997). The linear regime is often called the type I regime. It corresponds to a fast migration rate, although recent estimates (Miyoshi et al. 1999; Tanaka et al. 2002; Masset 2002) show that the linear analytical estimate assuming a flat two dimensional disk has to be reduced by a factor 2–3 or more in a more realistic calculation which accounts for the disk vertical structure and a possible non-saturation of the corotation torque if the disk is viscous enough. Migration in the type I regime is nevertheless still too fast, in the sense that the migration timescale it yields is shorter than the build-up timescale of a giant protocore (see e. g. Papaloizou & Terquem 1999). We shall not address this issue here but rather assume that a giant planet embryo can form in the disk at a distance  $r \geq 1$  AU, and with a mass  $M > M_{\rm crit}$ , where  $M_{\rm crit} \sim 15~M_{\oplus}$  is the critical mass above which rapid gas accretion begins.

When this embryo mass is large enough, it enters another well studied migration regime, called type II migration Ward (1997). In this regime, the protoplanet has a mass sufficient to open a gap in the disk, which is therefore split into an inner disk and an outer disk. The protoplanet then finds itself locked into the disk viscous evolution drifting inwards with it (Lin & Papaloizou 1986; Trilling et al. 1998). As the protoplanet undergoes type II migration towards the central object, it may accrete the surrounding nebula material. The accretion rate scales with the mass accretion rate onto the central object  $M_p \sim 3\pi\nu\Sigma$ , where  $\Sigma$  is the disk surface density. Here one assumes that the processes at work in the disk which contribute to the angular momentum exchange between neighboring rings can be adequately modeled by a phenomenological kinematic viscosity  $\nu$ . On the other hand, the type II migration timescale is of the order of the disk viscous timescale  $\tau_{\rm mig}^{\rm II} \sim \frac{r^2}{3\nu}$ . The maximum mass that a giant protoplanet can accrete on its way to the central object should be therefore of the order of  $M_p \sim \dot{M}_p \tau_{\rm mig}^{\rm II} \sim \pi r^2 \Sigma$ , that is of the order of the disk mass interior to the planet starting distance. Noticeably this mass does not depend on the disk viscosity. If the planet does not migrate all the way to the central object before the disk is dispersed, then because more time is spent at larger radii, it is most likely to be left with a semi-major axis larger than the typical one for hot Jupiters (0.05–0.2 AU, see Trilling et al. 2002). This is consistent with the observed paucity of planets with masses exceeding two Jovian masses at short periods (Zucker & Mazeh 2002). Note too that planets undergoing type II migration should tend to have higher masses at shorter periods. This is contrary to the observed trend. Furthermore, as the planet mass grows, it becomes eventually larger than the surrounding disk mass, and its migration rate tends to drop, as the disk cannot remove enough angular momentum from it. This has been investigated by Ivanov et al. (1999). In this case, the amount of time necessary to bring the planet to a close orbit can be considerably larger than the disk viscous timescale, and can even exceed the disk lifetime. This migration slowing can be seen in the simulations of Nelson et al. (2000). It occurs soon after the planet has entered its type II migration regime.

From the above considerations, it is questionable whether the orbital characteristics of most close orbiters can be accounted for by type II migration driven by the evolution of the disk. Furthermore the vast majority of these have sub-Jovian masses (here one excepts Tau Boo and GJ 86, which have large masses and which may have had a different origin). Depending on the physical conditions of the protoplanetary disks in which they formed, they may not have fulfilled the gap opening criteria (Lin & Papaloizou 1986, and references therein), with the consequence that they may have been involved in a migration regime intermediate between type I and type II.

This transitional regime has received little attention. Ward (1997) and Ward & Hourigan (1989) have worked out the feedback on the migration rate due to the nebula surface density

profile perturbation under the action of the protoplanet Lindblad torques. They introduced the concept of an inertial limit, that is the maximum mass of a protoplanet that can undergo steady state migration. It was suggested that masses above the inertial limit lead to a gap opening and to type II migration. In their analysis, Ward & Hourigan (1989) neglected the coordital dynamics and the corotation torque it implies on the migrating planet. The purpose of this work is to give an evaluation of the corotation torque for a migrating planet, and to analyze its consequences on migration. We define the notation in section 2, we present an appropriate expression for the corotation torque for a planet held on a fixed circular orbit in section 3, we then derive the corotation torque for a migrating planet in section 4, and illustrate its properties using customized numerical simulations in section 5. As we investigate the intermediate regime between type I and type II migration, for which the disk response is affected by non-linear effects, the Hill radius and the disk thickness have comparable orders of magnitude. The regime of interest thus involves mildly embedded protoplanets. We assume that it can be safely studied through two dimensional flat disk calculations provided a reasonable value is adopted for the gravitational potential smoothing length. In section 6 we demonstrate the existence of runaway migration and relate the condition for its occurrence to the analytic discussion in section 4. Finally in section 7 we summarize our results and we discuss their application to EGPs.

#### 2. Notation

We adopt a cylindrical coordinate system  $(r, \theta, z)$  centered on the primary, the origin of which corotates with the planet which is located at azimuth  $\theta = 0$ . We consider a thin gaseous disk with mid-plane at z = 0, with surface density  $\Sigma(r)$ , orbiting a central point-like object of mass  $M_*$ . The associated Keplerian frequency is  $\Omega_K(r) = \sqrt{GM_*/r^3}$ . In the unperturbed disk the orbital frequency is  $\Omega_0(r)$ , which is usually slightly smaller than  $\Omega_K(r)$  because the central acceleration is not only compensated for by the centrifugal acceleration, but also by a radial pressure gradient. The disk thickness is H(r) and the disk aspect ratio is h(r) = H(r)/r. In this disk we consider an embedded planet with mass  $M_p$  (we note  $q = M_p/M_* \ll 1$ ) and semi-major axis a. Its orbital frequency is  $\Omega_p = \Omega_K(a)$ . We shall restrict ourselves to the case where its eccentricity e can be neglected. We now write the angular frequency as  $\Omega(r,\theta) = \Omega_0(r) + v/r$ , and we denote by  $u(r,\theta)$  the radial velocity of the fluid element at  $(r,\theta)$ .

#### 3. Corotation torque for a planet on a fixed circular orbit

The link between the corotation torque and the horseshoe orbit drag has been indicated by Ward (1991, 1992). A torque estimate for a planet on a fixed circular orbit embedded in a viscous disk has been given by Masset (2001) who considered a steady flow as seen in the planet frame. We here derive an expression for the corotation torque in a disk with very small viscosity. Then the specific vorticity is conserved along a streamline (Balmforth & Korycansky 2001, and references therein).

We assume a steady flow in the planet frame. As we assume that the viscosity is low, we can write a Bernoulli invariant along a streamline:

$$J = \frac{u^2 + r^2(\Omega - \Omega_p)^2}{2} + \phi_{\text{eff}} + \eta,$$
 (1)

where  $\eta$  is the fluid specific enthalpy and  $\phi_{\text{eff}} = \phi - r^2 \Omega_p^2/2$ , with  $\phi$  being the gravitational potential. The Bernoulli invariant is a useful label of the librating streamlines in the horse-shoe region. The corotation torque expression, following Ward (1991), can be obtained by summing the contribution to the torque due to individual fluid elements over the horseshoe annular slab. The positive contribution coming from the outer fluid elements caught up by the planet, when they execute a U-turn in front of the latter, reads:

$$\Gamma^{+} = \int_{r_{c}}^{r_{c}+x_{s}} \Sigma(r_{+})r_{+}(\Omega_{p} - \Omega)[j(r_{+}) - j(r_{-})]dr_{+}, \tag{2}$$

where  $x_s$  is the horseshoe zone half-width,  $j(r) = r^2\Omega$  is the specific angular momentum,  $r_c$  is the corotation radius, and where we add an index +/- to any quantity to refer to its value on the outer/ inner part of its horseshoe streamline. The gradient of the Bernoulli invariant is linked to the flow vorticity (see e. g. Foglizzo & Ruffert 1997). If we denote by  $\omega$  the vertical component of the flow vorticity in the inertial frame, then we have:

$$\frac{\partial J}{\partial r} = r\omega(\Omega - \Omega_p),\tag{3}$$

where we use the fact that  $r\Omega^2 = \partial(\phi + \eta)/\partial r$ , and where we evaluate this expression sufficiently far from the planet so that we can assume u = 0 and so that we can neglect the dependency of J upon  $\theta$ . This allows one to transform Eq. (2) as:

$$\Gamma^{+} = -\int_{J(r_c)}^{J(r_c+x_s)} \frac{\Sigma(J)}{\omega} \gamma(J) dJ, \tag{4}$$

where we note  $\gamma(J) = j(r_+) - j(r_-)$  the specific angular momentum drop of a fluid element as it switches from the outer horseshoe leg to the inner one. If  $w = \Sigma/\omega$  is the inverse of the

specific vorticity, then:

$$\Gamma^{+} = 16|A_p|B_p^2 a \int_0^{x_s} w(x)x^2 dx,$$
 (5)

where  $A_p = (1/2)r\partial\Omega/\partial r$  and  $B_p = (1/2r)\partial(r^2\Omega)/\partial r$  are respectively the first and second Oort's constants, evaluated at the planet orbit. Here we assume that the planet mass is small enough that we can consider that a fluid element on an outer horseshoe leg at r = x + a is mapped on the inner leg with radius r = a - x, we have developed  $\gamma(x)$  to first order in  $x = [\gamma(x) = 4B_pax]$ , and we have assumed  $r_c = a$ . A similar treatment for the inner horseshoe leg yields the torque exerted on the protoplanet by the fluid elements which catch the planet up and are promoted to higher specific angular momentum orbits:

$$\Gamma^{-} = 16|A_p|B_p^2 a \int_0^{-x_s} w(x)x^2 dx.$$
 (6)

It should be noted that the corotation torque, in the non-linear regime (i. e. for  $x_s$  finite) should include all the fluid elements which corotate, in average, with the planet, that is to say all the fluid elements which librate in the corotating frame. This includes not only the horseshoe streamlines, but also the circumplanetary disk (corresponding to the closed streamlines interior to the Roche lobe). We find it more convenient to consider only the horseshoe drag exerted on the system {planet + circumplanetary disk}, considered as a whole, and hereafter the planet should be understood as this system.

#### 4. Corotation torque on a migrating planet

We shall now use Eq. (5) and (6) to evaluate the torque on a migrating object. We separate the orbital timescale  $O(\Omega^{-1})$  (which is also the horseshoe U-turn timescale from one leg to another) from the horseshoe libration timescale  $O(\Omega^{-1}a/x_s)$ , which is much longer. In particular, we neglect migration over the orbital timescale, while we consider it over the libration timescale. We say that migration is slow whenever the libration time of an outermost fluid element close to the separatrix between librating and circulating streamlines is short compared to the migration time across the horseshoe zone half width. As the former quantity is  $2\pi a/(|A_p|x_s)$  and the latter  $x_s/|\dot{a}|$ , the condition for slow migration reads:

$$|\dot{a}| \ll \frac{|A_p|x_s^2}{\pi a},\tag{7}$$

which is also, for a Keplerian disk:

$$|\dot{a}| \ll \frac{3}{2} \cdot \frac{x_s}{\tau_{\rm orb}} \cdot \frac{x_s}{a},\tag{8}$$

where  $\tau_{\rm orb} = 2\pi/\Omega$  is the orbital time scale. We assume that Eqs. (5) and (6) are still valid, provided care is taken about the evaluation of w(x). In particular, as the planet migrates, the "impact parameter" x = r - a of a fluid element varies as its azimuth varies. We therefore have to consider the outer incident fluid elements at an azimuth  $\theta_R \gtrsim 0$ . This azimuth needs to be small enough so that no significant radial drift occurs between the fluid element and the planet before the close encounter, and large enough so that the close encounter has not begun yet. Similarly, the azimuth at which the incident inner fluid elements need to be considered has to be  $\theta_L \lesssim 2\pi$ . We use the index R/L for the quantities relating to the close encounters originating from  $\theta_R \gtrsim 0 / \theta_L \lesssim 2\pi$ ). The positive part of the corotation torque is given by:

$$\Gamma_{+} = 16|A_{p}|B_{p}^{2}a \int_{0}^{x_{s}} w_{R}^{+}(x)x^{2}dx,$$
(9)

while the negative part of the corotation torque is given by:

$$\Gamma_{-} = 16|A_p|B_p^2 a \int_0^{-x_s} w_L^{-}(x) x^2 dx. \tag{10}$$

Note that we assume the value of  $x_s$  to be the same as in the non-migrating case. Although this needs to be reconsidered for a significant drift rate, this is surely true as long as migration is slow (with the meaning defined earlier in this section). The numerical simulations presented in the next section will be used to check this assumption. The sum of Eqs. (9) and (10) can be transformed so that values of  $w_L(x)$  and  $w_R(x)$  on the same side of the orbit are considered. Care has to be taken about the sign of  $\dot{a}$  before making this transformation. We shall assume hereafter that  $\dot{a} < 0$ . Hence:

$$\Gamma = 16|A_p|B_p^2 a \int_{-x_c}^0 [w_R^-(x) - w_L^-(x)]x^2 dx, \tag{11}$$

where we use the fact that  $w_R^+(x) = w_R^-(-x)$  for any x in  $[-x_s, +x_s]$ , since all of the fluid elements which execute a right U-turn are trapped in the coorbital region (see also Figs. 16 and 17 in appendix A).

We shall now temporarily assume a steady migration case  $(\ddot{a} = 0)$ . We call  $f: x \mapsto y$  the mapping of a fluid element, between two close encounters with the planet. This notation is illustrated in Fig. 1. Consider a fluid element initially located at the distance x of the orbit just after a close encounter. Its distance to the orbit just before the next close encounter is:

$$y = f(x) = x + \frac{\pi a}{|A_p|x}\dot{a},\tag{12}$$

where we assume that  $y \simeq x$  (i. e. slow migration). Within this approximation, the reciprocal map  $f^{-1}$  reads:

$$x = f^{-1}(y) = y - \frac{\pi a}{|A_p|y}\dot{a}.$$
 (13)

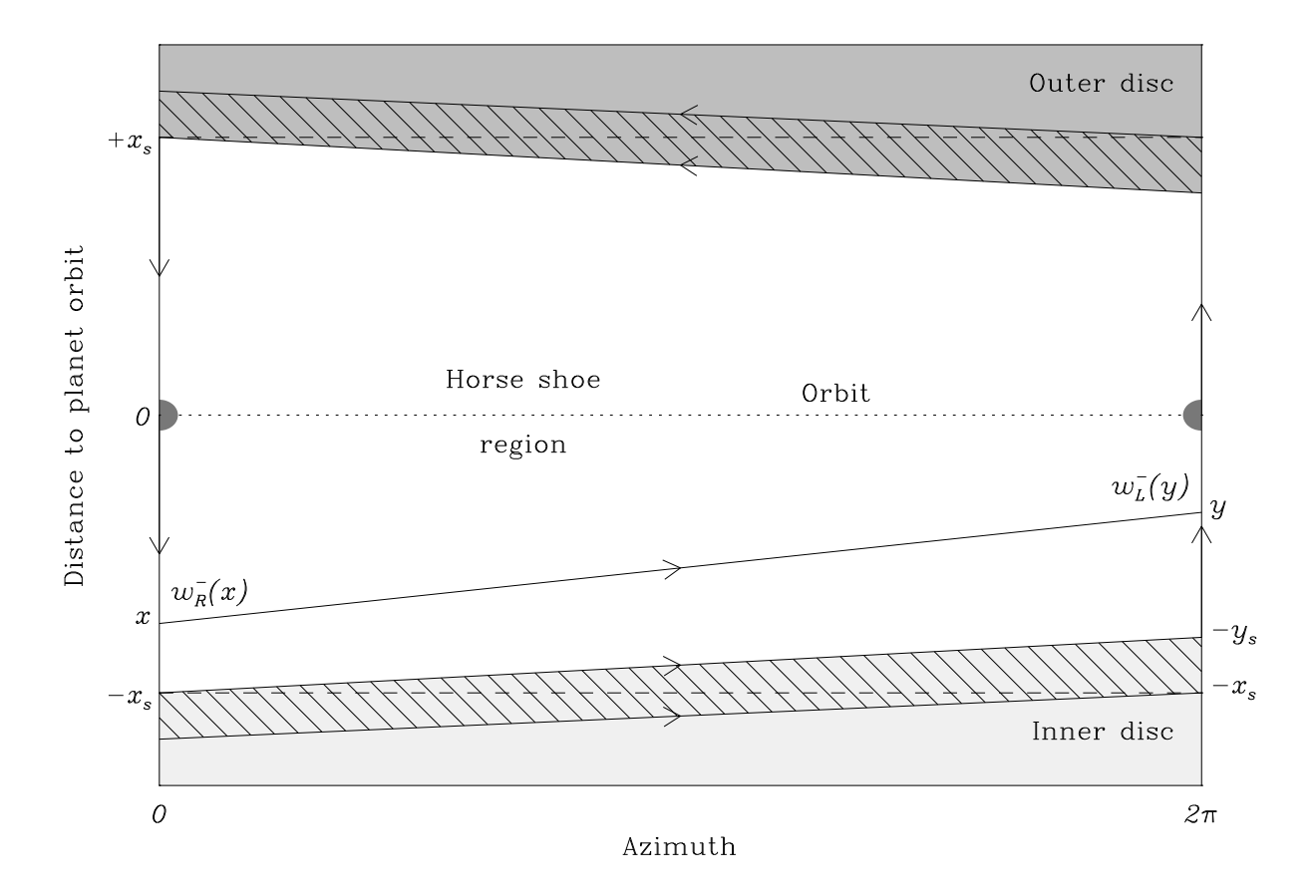


Fig. 1.— Sketch of a fluid element path for a situation with  $\dot{a} < 0$ . The planet is orbiting to the right. It is located at  $\theta = 0 \pmod{2\pi}$ . The fluid elements paths are represented in a  $(\theta, x = r - a)$  plane. The separatrices are represented by dashed lines. The distance to the orbit of the fluid element is initially x (just after a R-close encounter) and is y after a half libration time (just before a L-close encounter). The bottom hashed zone represents the material from the inner disk that will have crossed the inner separatrix before the next close encounter. Therefore this material participates once in the corotation torque, and then flows out of the horseshoe region at the outer separatrix and circulates in the outer disk.

Because of the conservation of specific vorticity, one can write:  $w_R^-(x) = w_L^-(y)$ , for any x in  $[-x_s, 0]$ . Eq. (11) therefore reads:

$$\int_{-x_s}^{0} w_R^{-}(x) x^2 dx = \int_{-y_s}^{0} w_L^{-}(y) \left( y - \frac{\pi a \dot{a}}{|A_p| y} \right)^2 \times \left( 1 + \frac{\pi a \dot{a}}{|A_p| y^2} \right) dy, \tag{14}$$

where  $y_s = f(x_s)$ , and where we have taken x = y = 0 as an upper limit for both integrals, since the contribution of material close to the orbit is vanishingly small for slow migration<sup>2</sup>. Expanding the integrand to first order in  $a\dot{a}/(|A_p|y^2)$ , one can write the corotation torque given by Eq. (11) as:

$$\Gamma_{\rm sm} = 16|A_p|B_p^2 a \left[ \int_{-y_s}^0 w_L^-(y) y^2 \left( 1 - \frac{\pi a \dot{a}}{|A_p|y^2} \right) dy - \int_{-x_s}^0 w_L^-(x) x^2 dx \right], \tag{15}$$

where the sm index stands for "steady migration". Eq. (15) can be transformed into:

$$\Gamma_{\rm sm} = 16|A_p|B_p^2 a \left[ -\int_{-y_s}^0 w_L^-(y) \frac{\pi a \dot{a}}{|A_p|} dy - \int_{-x_s}^{-y_s} w_L^-(x) x^2 dx \right].$$
(16)

The first integral (over y, from  $-y_s$  to 0) corresponds to the material which librates in the horseshoe region (white trapezoidal area in Fig. 1). The corresponding torque expression is:

$$\Gamma_1 = -16\pi B_p^2 a^2 \dot{a} \int_{-y_s}^0 w_L^-(y) dy$$
$$= -2B_p a \dot{a} M_{\text{coorb}}, \tag{17}$$

<sup>&</sup>lt;sup>2</sup>More precisely, the material at low |x| is not mapped onto y, and one should write  $-x_T$  as an upper limit of the L.H.S. integral of Eq. (14) instead of 0, where  $-x_T$  is defined by  $f(-x_T) = 0$ . One finds  $x_T^2 = 8\pi a\dot{a}/(3\Omega)$ . The contribution of material in the  $[-x_T, 0]$  region is therefore  $\sim (1/3)w_R(0)x_T^3$ , and scales therefore as  $\dot{a}^{3/2}$ , whereas the effect of migration on the corotation torque is in  $\dot{a}$ . The relative contribution of this innermost material is therefore vanishingly small for slow migration, and it is safe to write 0 as an upper limit for the L.H.S. integral.

where  $M_{\text{coorb}}$ , the "vorticity weighted coorbital mass", is defined as:

$$M_{\text{coorb}} = 4\pi a B_p \int_{-y_s}^{0} \frac{\Sigma_L(y)}{B(y)} dy$$
$$= 4\pi a B_p \int_{-x_s}^{0} \frac{\Sigma_R(x)}{B(x)} dx. \tag{18}$$

This component  $\Gamma_1$  of the torque arises because the librating fluid elements migrate radially with the planet and have to lose specific angular momentum at the same rate as this latter. For the case of an inward migration, the torque exerted on this region by the planet is negative. It exerts therefore a positive torque on the planet, and thus has a negative feed back on migration. A similar conclusion applies for the case of an outwards migration.

The second integral in Eq. (16) can be evaluated assuming  $y_s \approx x_s$  (i. e. slow migration), in which case it reduces to:

$$\Gamma_2 = -16|A_p|^2 B_p^2 a(x_s - y_s) w_L(-x_s) x_s^2$$

$$= 8\pi B_p^2 a^2 x_s \dot{a} \frac{\Sigma(-x_s)}{B(-x_s)}.$$
(19)

As this torque corresponds to the integral over  $-x_s < y < -y_s$ , it comes from the fluid elements of the hashed area of Fig. 1. These fluid elements are promoted to higher specific angular momentum trajectories after their (unique) close encounter with the planet. For the case of inwards migration, they therefore contribute negatively to the corotation torque and hence exert a positive feed back on migration.

When one adds Eqs. (17) and (19), one gets the following torque expression:

$$\Gamma = 2B_p a \,\delta m \,\dot{a},\tag{20}$$

where we introduce the "vorticity weighted coorbital mass deficit" defined as:

$$\delta m = 8\pi a \left[ x_s w_R(-x_s) - \int_{-x_s}^0 w_R(x) dx \right] B_p$$

$$= 4\pi a \left[ x_s \frac{\Sigma_R(-x_s)}{B(-x_s)} - \int_{-x_s}^0 \frac{\Sigma_R(x)}{B(x)} dx \right] B_p. \tag{21}$$

If one neglects the radial variation of B(x) across the horseshoe region, the coorbital mass deficit appears as the mass difference between the mass of the horseshoe region, if the material in it had everywhere the surface density that it has at the inner separatrix, with its actual mass. As the coorbital region is generally depleted, this coorbital mass deficit is positive.

One can then get an estimate of the torque for a non-steady migration using the following simple argument: if  $\dot{a}$  varies, the mass flux across the upstream separatrix varies, and this will have an impact on the torque exerted on the planet when the deficit or excess of inflowing mass w.r.t. a steady state situation undergoes a close encounter with the planet, i. e. after a characteristic time equal to  $\tau_{\text{lag}} = \tau(x_s)/2$ , where  $\tau = (\pi a/|A_p|)|x|^{-1}$  is half the libration time, i. e. the time a fluid element at a distance |x| from the orbit needs to go from azimuth  $\theta_R \approx 0$  to azimuth  $\theta_L \approx 2\pi$ . Therefore  $\tau_{\text{lag}}$  is the time that a fluid element opposite the planet needs to drift to attain conjunction with it. One can therefore write:

$$\Gamma = \Gamma_{\rm sm}[\dot{a}(t - \tau_{\rm lag})]$$

$$= \Gamma_{\rm sm}(\dot{a}) - \tau_{\rm lag}\ddot{a}\frac{d\Gamma_{\rm sm}}{d\dot{a}}$$

$$= 2B_p \,\delta m \,a\dot{a} - \frac{\pi a^2 B_p}{|A_p|x_s} \,\delta m \,\ddot{a}. \tag{22}$$

An exact method to evaluate the  $\ddot{a}$  term in the slow migration limit, when one knows the specific vorticity profile across the horseshoe region, is provided in appendix A. It can be noted that this torque expression cancels out for a planet held on a fixed circular orbit  $(\dot{a} = \ddot{a} = 0)$ . This is expected as we have used  $w_R^-(-x) = w_R^+(x)$ , i. e. that the specific vorticity is conserved along a streamline. Hence in the absence of migration, the torque is saturated. We could have used another dependency of  $w_R^-(-x)$  on  $w_R^+(x)$ , involving a radial gradient of specific vorticity, which would have led to a constant term which we would interpret as the "static" part of the corotation torque. However, as our concern is to capture the planet drift effects on the torque, this would not have brought further insight regarding the runaway process we aim at characterizing.

We note  $\Delta\Gamma_{LR}$  the other torque that is applied to the planet, which corresponds to non-librating (i. e., circulating) material, which we assume to correspond to the differential Lindblad torque. Assuming that migration occurs with a negligible eccentricity, we have:

$$2B_p a M_p \dot{a} = \Gamma + \Delta \Gamma_{LR}. \tag{23}$$

This takes also the following form:

$$2B_p a(M_p - \delta m)\dot{a} = \Delta\Gamma_{LR} - \frac{\pi a^2 \delta m B_p}{x_s |A_p|} \ddot{a}, \qquad (24)$$

which also takes the following form in the Keplerian case:

$$a\frac{\Omega_p}{2}(M_p - \delta m)\dot{a} = \Delta\Gamma_{LR} - \frac{\pi a^2 \,\delta m}{3x_s}\ddot{a}.$$
 (25)

Assuming that the  $\dot{a}$  variations, if any, occur on a time interval short enough to consider a as a constant, one gets two different behaviors from Eq. (24):

1.  $M_p > \delta m$ : the coorbital mass deficit is smaller than the planet mass, which is the case either for sufficiently low planet masses or for a large planet mass, when the planet mass is comparable to or larger than the surrounding disk. In that case the coorbital mass deficit cannot become larger than the planet mass. Then the corresponding homogeneous equation indicates that disturbances to a are damped on the short timescale

$$\tau_d \simeq \tau_{\rm orb} \frac{a}{x_s} \frac{\delta m}{M_p - \delta m}.$$
(26)

One can therefore discard transient behavior, retaining only the standard first order ODE for migration:

$$a\frac{\Omega_p}{2}(M_p - \delta m)\dot{a} = \Delta\Gamma_{LR},\tag{27}$$

where the only difference with the usual expression is that we replace the planet mass alone  $M_p$  by the "planet effective mass"  $m_{\text{eff}} = M_p - \delta m$ .

2.  $M_p < \delta m$ : the planet mass is large enough to open a significant dip in the disk, and this latter is substantial enough for the coorbital mass deficit to be larger than the planet mass. In that case the homogeneous ODE associated to Eq. (24) indicates that small perturbations to a are exponentially growing on a timescale  $\tau_d$ , which although depending on the exact value of  $|M_p - \delta m|/M_p$ , is of the order of a few tens of orbital periods (assuming, as is reasonable for a mildly embedded object in a typical protoplanetary disk, that  $x_s \sim 0.1$ ). The assumptions that we made to derive of Eq. (22), namely migration slow enough that the dip profile drifts instantaneously with the planet, and slow enough that the horseshoe zone crossing time is much larger than the libration time, rapidly break down, and one can only say at this point that this runaway regime is extremely fast, and that it occurs for  $\delta m > M_p$ . The actual behavior of a protoplanet in this regime has to be assessed through numerical simulations. Since the ultimate sign of  $\ddot{a}$  depends on the initial values of a and  $\dot{a}$ , runaway can in principle occur outwards under specific initial conditions which need to be specified.

#### 5. Numerical simulations

## 5.1. Code description

We performed a series of dedicated numerical simulations to test the runaway regime and the validity of Eq. (27). The code that we used has already been described elsewhere (see e. g. Nelson et al. 2000). As this code is an Eulerian grid-based code, it must fulfill the Courant condition on the timestep to ensure numerical stability. An improved algorithm

resulting in a less demanding CFL condition, with the average azimuthal velocity at each radius subtracted out (Masset 2000a,b) was used in order to increase the time step and speed up the code. The grid corotates with the guiding center of the planet osculating orbit. As a result, the planet motion with respect to the grid is slow, and mainly corresponds to a radial drift. Our rotating frame is angularly accelerated. The corresponding acceleration, that is  $\vec{r} \times \dot{\Omega}_p \vec{e_z}$ , is applied in much the same way as Kley (1998) handles the Coriolis acceleration in a rotating frame, so as to enforce angular momentum conservation. As these dedicated runs involve as accurate as possible a torque evaluation, we used non-reflecting boundary conditions so as to eliminate any reflected wave (which can bring back to the planet the angular momentum previously removed from it) and we used an initial profile with uniform specific vorticity (i. e. with  $\Sigma \propto r^{-3/2}$ , which leads to a constant drift rate  $\dot{a}$  up to the center, if one only considers the differential Lindblad torque). Our mesh consists of 450 sectors equally spaced in azimuth, divided radially in 143 zones, the successive radii of zone boundaries being in geometric progression.

## 5.2. Units and Setup

Our unit of mass is the central object mass  $M_*$ , our unit of length is the initial planet semi-major axis  $a_0$  and our unit of time is  $\Omega_K(a_0)^{-1}$ . In this system of units, the gravitational constant is therefore G = 1. The mesh outer boundary lies at  $2.5a_0$  and the inner boundary at  $0.4a_0$ . We use a uniform aspect ratio disk with  $h(r) \equiv 0.03$ . The resolution of our mesh is barely sufficient to accurately describe the differential Lindblad torque acting on the planet. On the other hand, it is enough for a proper description of coorbital effects (Masset 2002). Our planet mass is  $M_p = 3 \cdot 10^{-4}$  (which corresponds to a Saturn mass planet if the central star has a solar mass). We used a number of disk surface density profiles

$$\Sigma(r) = S_n \cdot 10^{-4} \cdot r^{-3/2} \tag{28}$$

with the following values  $S_0 = 0.5$ ,  $S_1 = 1$ ,  $S_2 = 1.5$ ,  $S_3 = 2$ ,  $S_4 = 3$ ,  $S_5 = 5$ ,  $S_6 = 8$ ,  $S_7 = 12$  and  $S_8 = 20$ . We used a uniform kinematic viscosity  $\nu = 10^{-5}$  throughout the disk. The planet was initially held on a fixed circular orbit for 477 orbits (t = 3000) in order to give it a sufficient time to open a dip/gap around its orbit. This creates a depression of the specific vorticity profile which can lead to the effect we described in section 2. It should be noted that the coorbital mass deficit that arises during the first 477 orbits just scales with the disk surface density, that is to say:  $\delta m \propto \Sigma_0$ , where  $\Sigma_0 = \Sigma(a_0)$ . Eq. (27) can therefore be written as:

$$(M_p - K\Sigma_0)\dot{a} = K'\Sigma_0 \tag{29}$$

where the constants K and K' both depend on  $M_p$  and the disk parameters, but this dependency does not need to be considered here as we only vary the disk surface density in these runs. Eq. (29) can be written as:

$$\dot{a}^{-1} = A(\Sigma_0^{-1} - \Sigma_{\text{crit}}^{-1}) \tag{30}$$

where we introduce the critical surface density  $\Sigma_{\rm crit}$  for migration runaway, with A being a proportionality constant which is simply related to the differential Lindblad torque, as one can see by letting  $\Sigma_0 \to 0$ . The novelty here is that the migration rate below the runaway limit grows faster than linearly with the disk surface density. Our simulations aim at testing this super-linearity by checking whether the drift rate fulfills Eq. (30) or not. When it does, we determine the critical disk surface density for runaway and determine whether we indeed get a runaway for larger surface densities. We also check that the critical surface density so determined is consistent with coorbital mass deficit estimates.

#### 5.3. Smoothing issues

The protoplanet potential in the runs presented here is smoothed using a softening parameter  $\varepsilon = \eta H$ , where H is the disk thickness and  $\eta = 0.6$ . The results turn out to be sensitive to the value of the softening parameter because the horseshoe zone width crucially depends on it. Lowering the softening parameter moves the separatrices away from the orbit. As a result, the coorbital mass deficit is increased, and the critical surface density for runaway is reduced. However, sensitivity to the softening parameter in a numerical simulation does not necessarily imply that the region within the Roche lobe matters, but rather that coorbital processes matter, as their effectiveness depends strongly on the horseshoe zone width which is linked to it (see Masset 2002, § 5 for details). Note that the discussion of the softening parameter by Masset (2002) is valid only for the case when the specific vorticity has a linear dependence on the distance to corotation (in which case the corotation torque scales as  $x_s^4$ ). Here the specific vorticity profile has a depleted, more complex profile, and the analysis is no longer valid. We used a softening parameter comparable to the one derived by Masset (2002), which was found to give reasonable results for the case of mildly embedded planets. It should be kept in mind that if a smaller softening parameter is used, the critical surface density for runaway that we shall discuss later would be even lower than what we found. In that sense the extent of the runaway regime that we shall delineate later in this work can be considered as a conservative estimate.

#### 5.4. Results

We show the temporal behavior of the planet semi-major axis for our nine runs at Fig 2. The origin of time is chosen at the planet release. The first 477 orbits are therefore not shown. One can already notice that the radial drift rate is not proportional to the disk mass. The heaviest disk is indeed "only" 40 times heavier than the lightest one we consider. For the lightest disk the planet migrates about  $\sim 1.5 \%$  inwards over 250 orbits, whereas for the heaviest disk the planet is already at r = 0.5 after about 20 orbits. Fig. 3 shows the migration rate as a function of time. We see that it is relatively constant for the runs  $S_0$ to  $S_4$ , that a slight global variation can be seen for the run  $S_5$ , and that the other runs,  $S_6$ to  $S_8$ , display a strongly variable migration rate, which peaks at very large values. Some oscillations in the migration rate for  $S_0$  to  $S_6$  can be seen. These can be identified with the planet crossing the boundaries of mesh zones (i. e. the period for these oscillations is  $|\Delta r/\dot{a}|$ , where  $\Delta r$  is the radial zone size, which explains why these oscillations are slower for the smaller migration rates). This also gives us an idea of the accuracy of the numerical scheme and of the torque dependency on the planet placement with respect to a mesh zone. This accuracy is satisfactory except for the run  $S_6$  which exhibits large amplitude variations, but these are likely not relevant since the planet is then close to the grid inner boundary. We can check that the drift rate grows faster than linearly with the disk surface density for runs  $S_0$  to  $S_5$ . We estimate the average migration rate for these runs, over the whole time interval for runs  $S_0$  to  $S_4$ , and over the time interval 40 to 80 orbits for the run  $S_5$  (we discuss this choice later). Fig. 4 shows  $|\dot{a}|^{-1}$  as a function of  $\Sigma^{-1}$ . The points are relatively well aligned, as was expected from Eq. (30). A linear regression fit allows one to determine the critical surface density for runaway, and yields  $S_{\text{crit}} = 6.7$ . The runs  $S_6$  to  $S_8$ , which correspond to disk surface densities larger than this runaway threshold, do indeed exhibit a very fast migration and a strongly time variable migration rate. One can also understand the time behavior of the drift rate in the first orbits of Fig. 3. As can be seen in Eq. (26), the timescale  $\tau_d$ , over which the migration rate tends to its limiting value given by Eq. (27), increases when the disk surface density approaches its critical value. This is precisely the trend that we see in our runs. This is the reason we took 40 orbits as a lower time value for estimating the average migration rate for run  $S_5$ . The higher time value of 80 orbits comes from the fact that by then the planet has already migrated a sizable fraction of its initial distance to the star such that its coorbital mass deficit may have been significantly altered.

We finally check whether the critical surface density corresponds to a coorbital mass deficit comparable to the planet mass. We display at Fig. 5 the surface density in the coorbital region (in a  $\theta$ , r-plane) and we superimpose a few streamlines. This allows us to get an estimate of the position of the separatrices, which we find at  $x_s \approx \pm 0.1a_0$ . Once one knows the location of the separatrices, one can estimate the coorbital mass deficit. Fig. 6

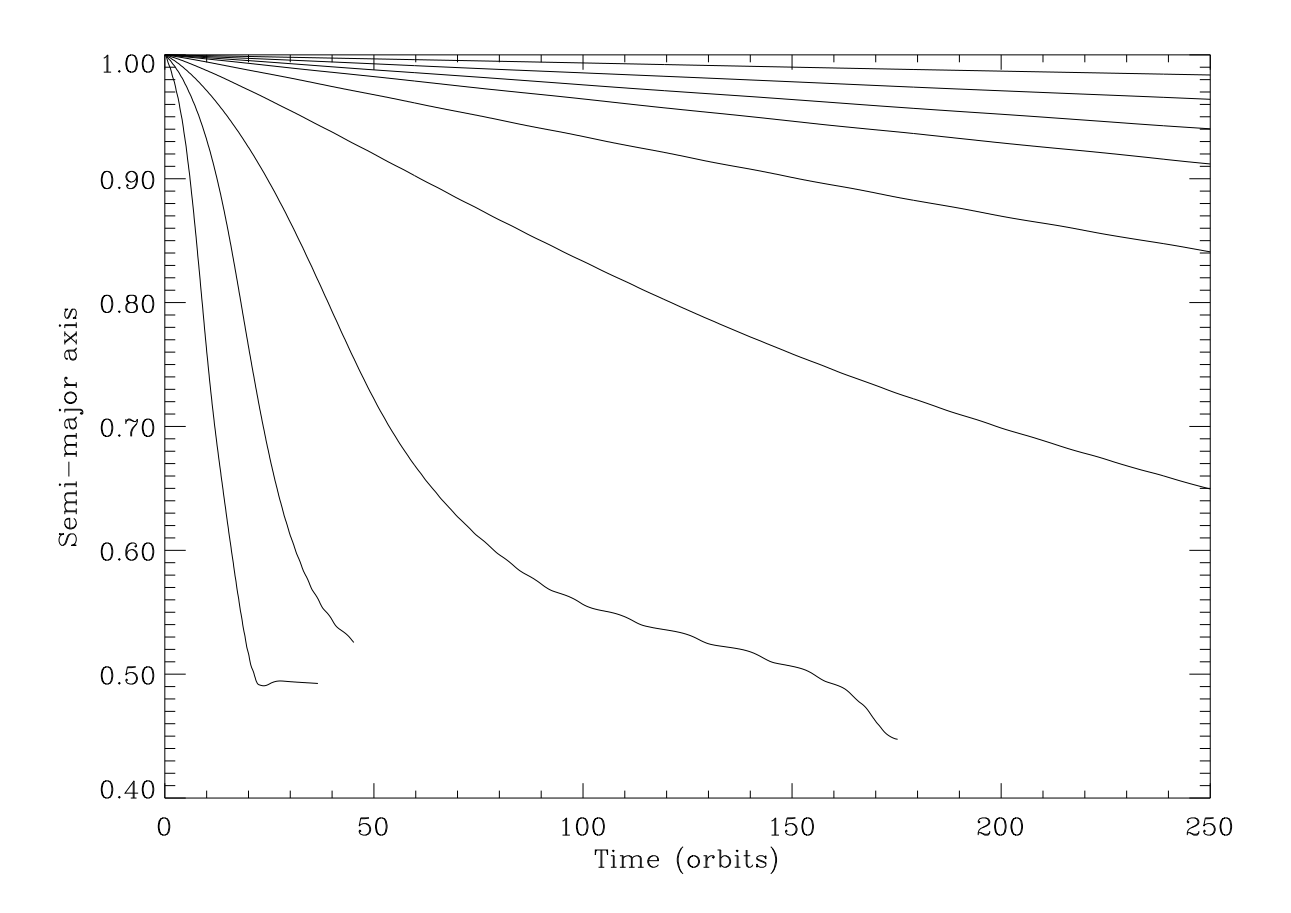


Fig. 2.— Semi-major axis as a function of time, for the different values of  $S_n$ , n ranging from 0 to 8 from top to bottom. The behavior is meaningless when a gets close to the grid inner boundary, located at  $R_{\min} = 0.4$ .

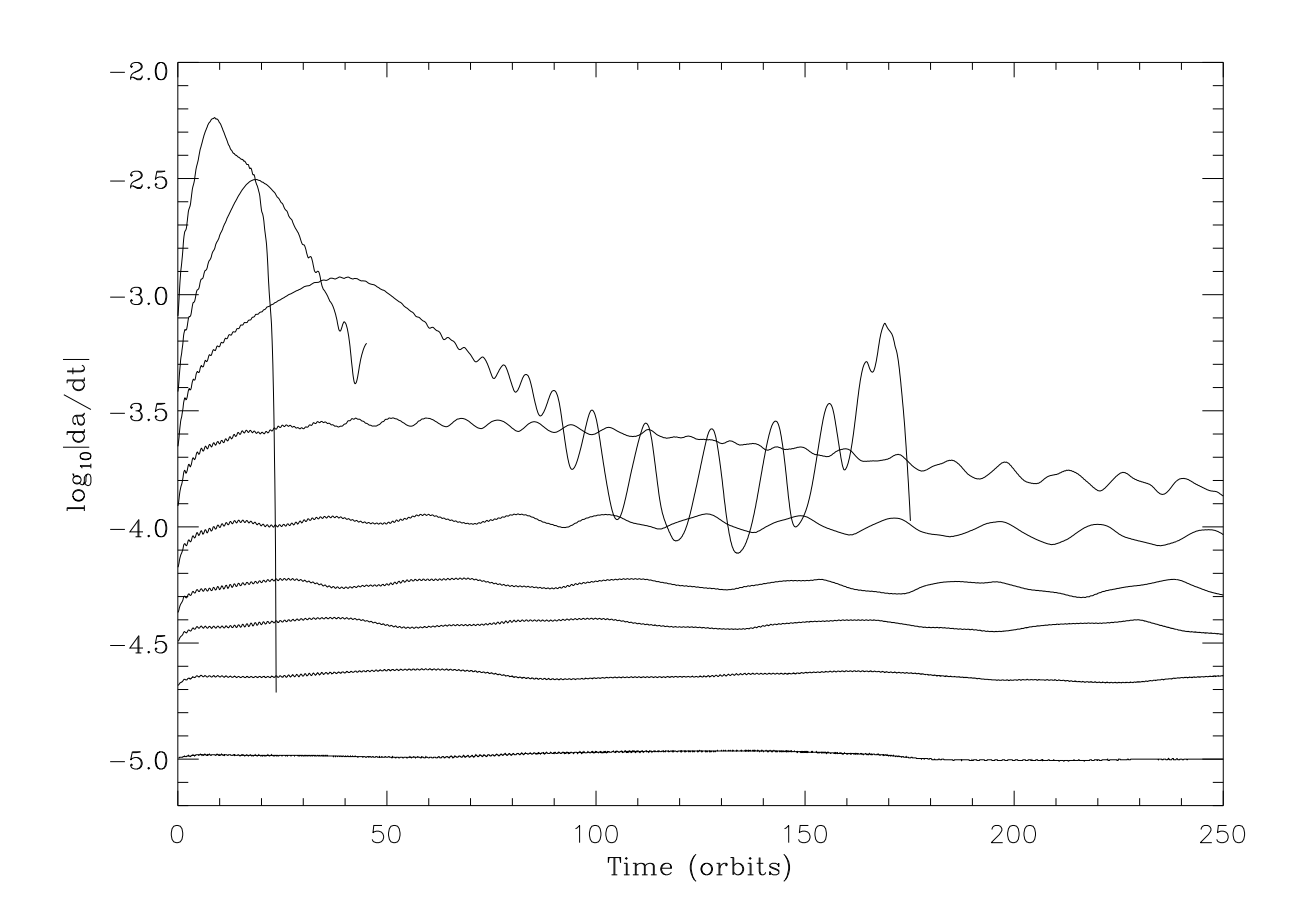


Fig. 3.— Drift rate as a function of time. n ranges from 0 to 8 from bottom to top.

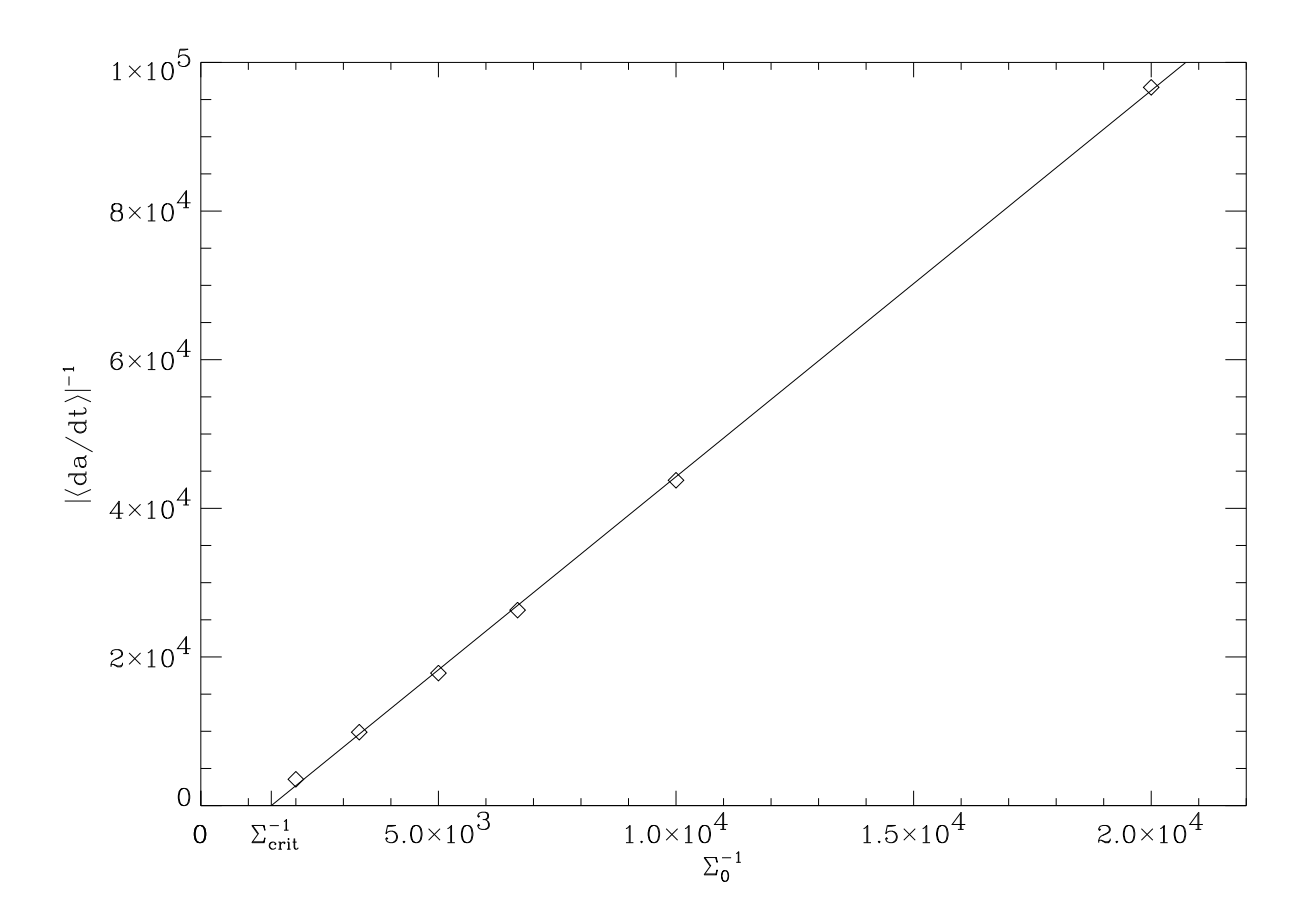


Fig. 4.— Inverse of average drift rate as a function of the inverse of disk surface density.

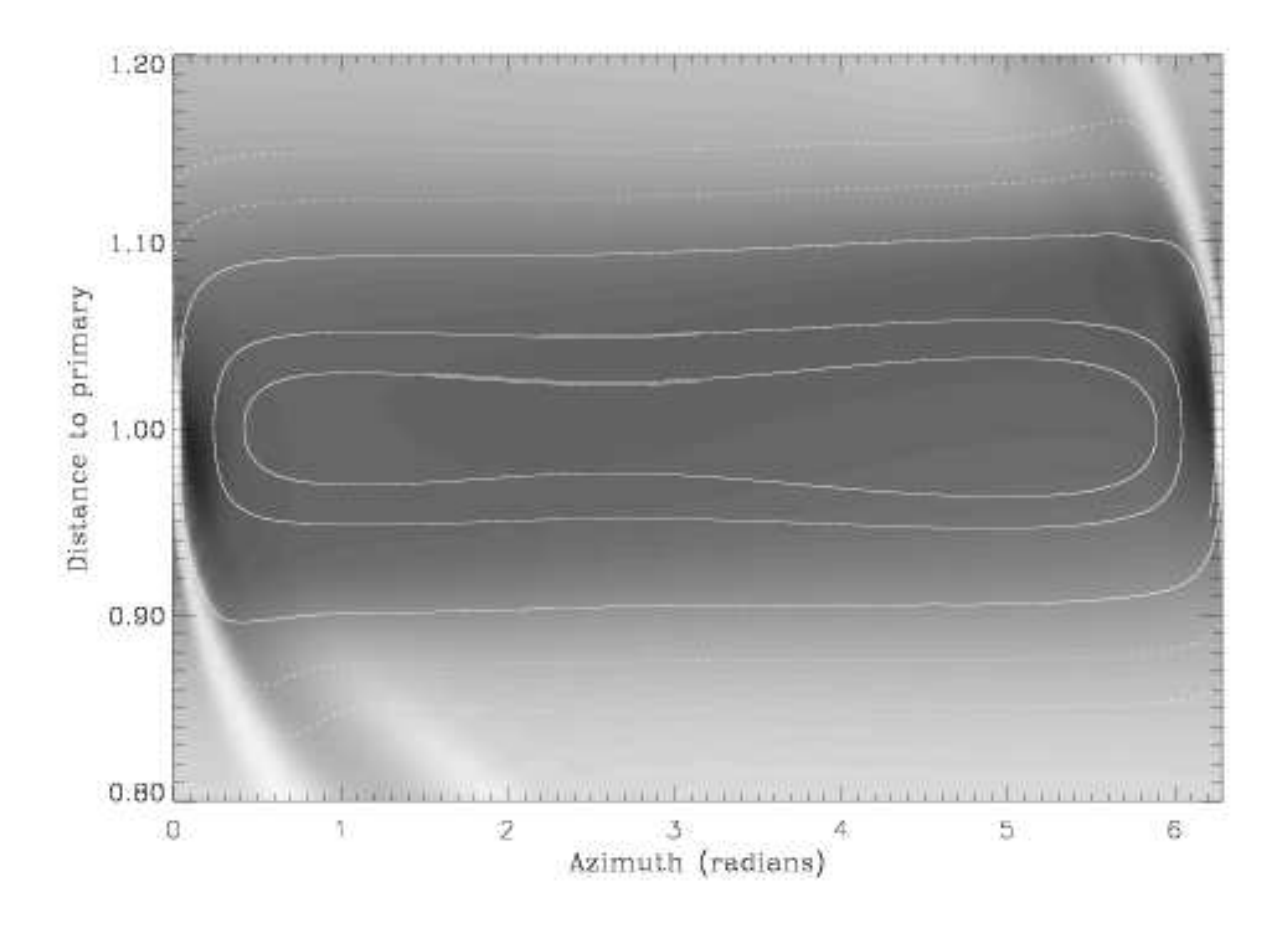


Fig. 5.— Surface density and streamline aspect for any run  $S_0$  to  $S_8$  just before the planet is released. The circulating streamlines are dotted, while the librating ones are solid.

shows the inverse specific vorticity profile for run  $S_1$ , from which one can estimate a coorbital mass deficit  $\delta m = 3.44 \cdot 10^{-5}$ . This latter needs therefore to be  $M_p/\delta m = 8.7$  times more massive to fulfill the runaway condition, from which we conclude that the runaway should occur for S = 8.7. This value is 30 % larger than the value inferred from the linear regression fit. The agreement is not surprisingly rough, probably owing to the various assumptions made to derive Eq. (21).

#### 5.5. Additional runs

In addition to the main runs involving freely migrating planets, we have performed a series of additional runs in which the migration rate  $\dot{a}$  is fixed in order to check the behavior described by Eq. (22). Namely, in these runs, the planet was held on a fixed  $\dot{a}$  trajectory for 200 orbits. The run was started with semi major axis  $a_0 = 1 - 150 \cdot 2\pi \dot{a}$  and ended with semi major axis  $a_1 = 1 + 50 \cdot 2\pi \dot{a}$ , so that in all the runs the planet has semi major axis a = 1 at t = 150 orbits. The planet is given an instantaneous orbital frequency equal to  $\Omega_K(a)$ . The runs are performed as before in the frame corotating with the guiding center. The resolution and other numerical values are unchanged with respect to what is described in the previous section. The values adopted for  $\dot{a}$  are  $\dot{a} = D \times 5 \cdot 10^{-5}$ , where D is an integer ranging from -3 to +6. The surface density in all these runs is  $\Sigma_0 = 10^{-4}$ , corresponding to S = 1.

Fig. 7 shows the torque as a function of time for each of the ten runs performed, and Fig. 8 shows the average value of the torque as a function of  $\dot{a}$  (the average is taken over the time interval [100, 200] orbits, which eliminates initial transient behavior occurring over the first 100 orbits, and which ensures that the average semi major axis of the planet over this time interval is the same for all the runs, and is  $\bar{a} = 1$ .)

The torque modulation as the planet sweeps radially the mesh zones is again apparent in Fig. 7. These plots confirm the linear dependence of the total torque upon the migration rate. One can check that the slope of  $\Gamma$  as a function of  $\dot{a}$  is positive, i. e. the feed back is positive, and one can infer from the slope estimate the critical disk surface density for runaway. We note  $\gamma = \Gamma/M_p$  the specific torque acting on the planet. We can write, since  $\ddot{a} = 0$ :

$$\gamma_{\text{tot}} = \gamma + \Delta \gamma_{\text{LR}} 
= 2B_p a \dot{a} \frac{\delta m}{M_p} + \Delta \gamma_{\text{LR}}.$$
(31)

We also have the relationship:

$$\delta m = M_p \Sigma / \Sigma_{\text{crit}},\tag{32}$$

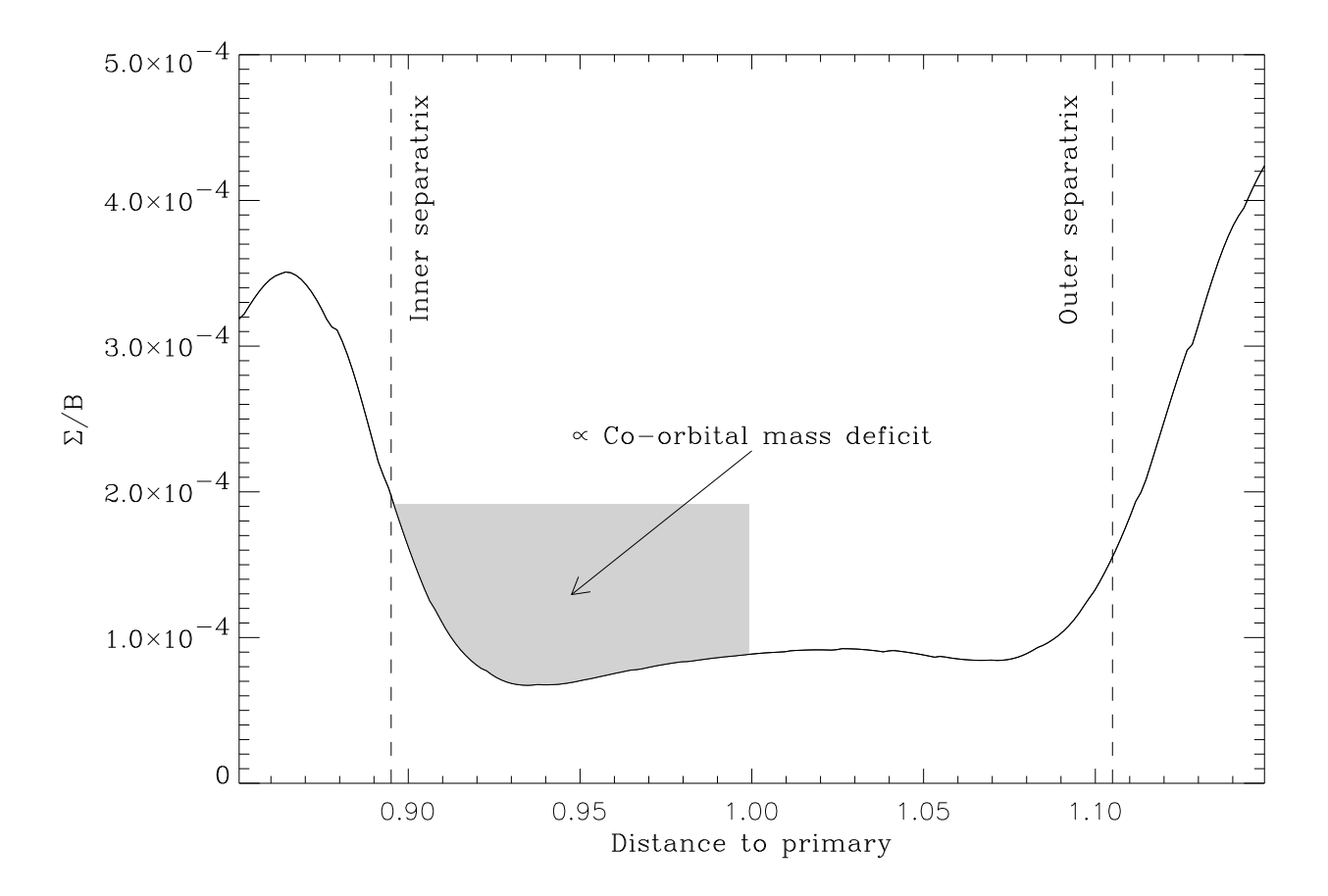


Fig. 6.— Coorbital mass deficit estimate from run  $S_1$ . As can be seen the profile is depleted in the coorbital region. The coorbital mass deficit is related to the shaded area. The profile is relatively symmetric inside of the coorbital region, which indicates that the corotation torque is saturated (cancels out) in the absence of migration. The inner separatrix position is  $x_s = -0.105$ . The coorbital mass deficit, as shown here, has to be evaluated from the depleted profile shape between the orbit and the upstream separatrix. For the case of an outwards migration the right part of the profile should have been used. As we consider in this case a  $\Sigma \propto r^{-3/2}$  profile, this would make no difference as the unperturbed specific vorticity profile is flat.

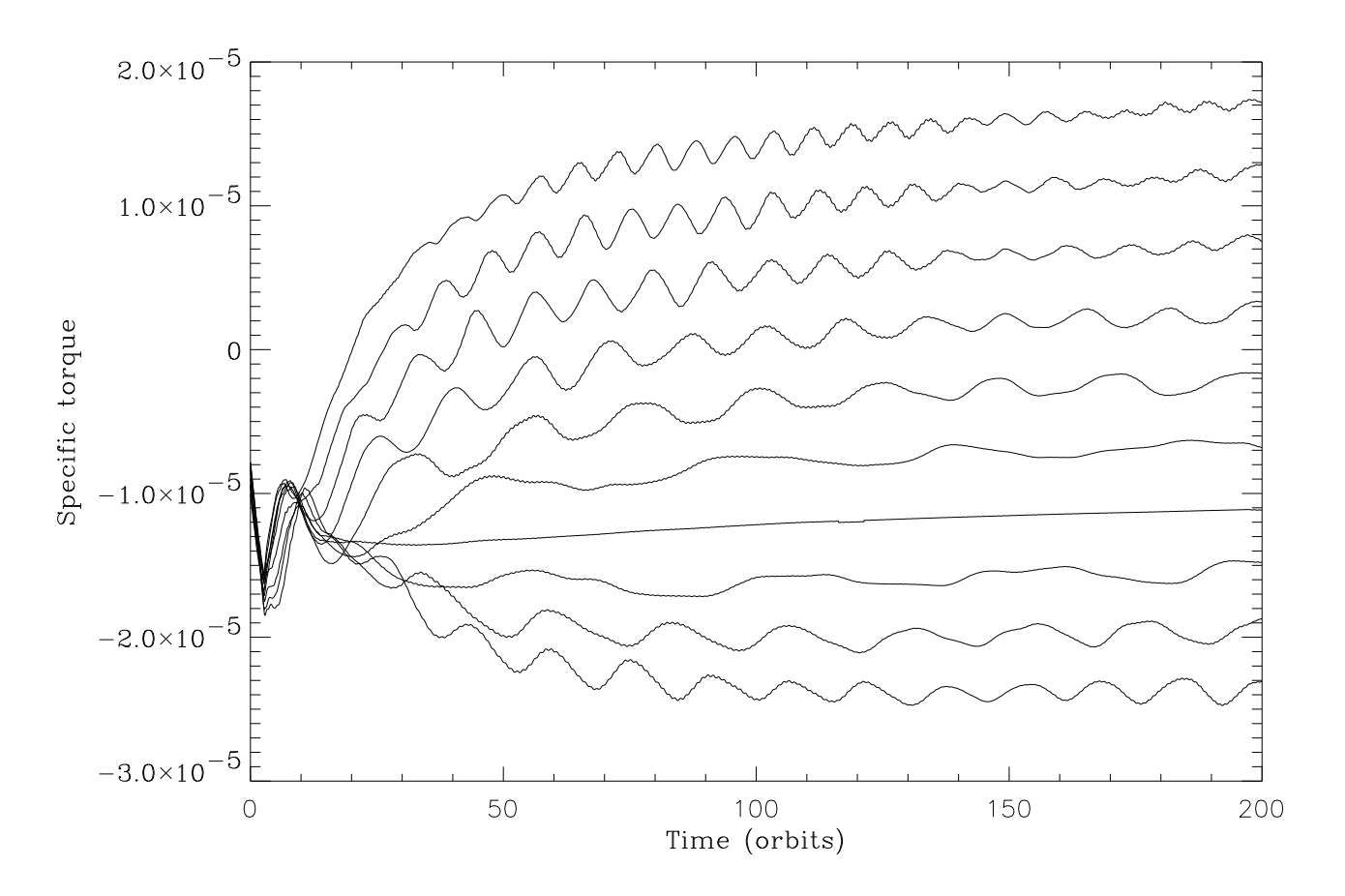


Fig. 7.— Measured total specific torque value (smoothed over a 5 orbit temporal window) as a function of time, for runs D = -3 to +6. The value of D increases from bottom to top.

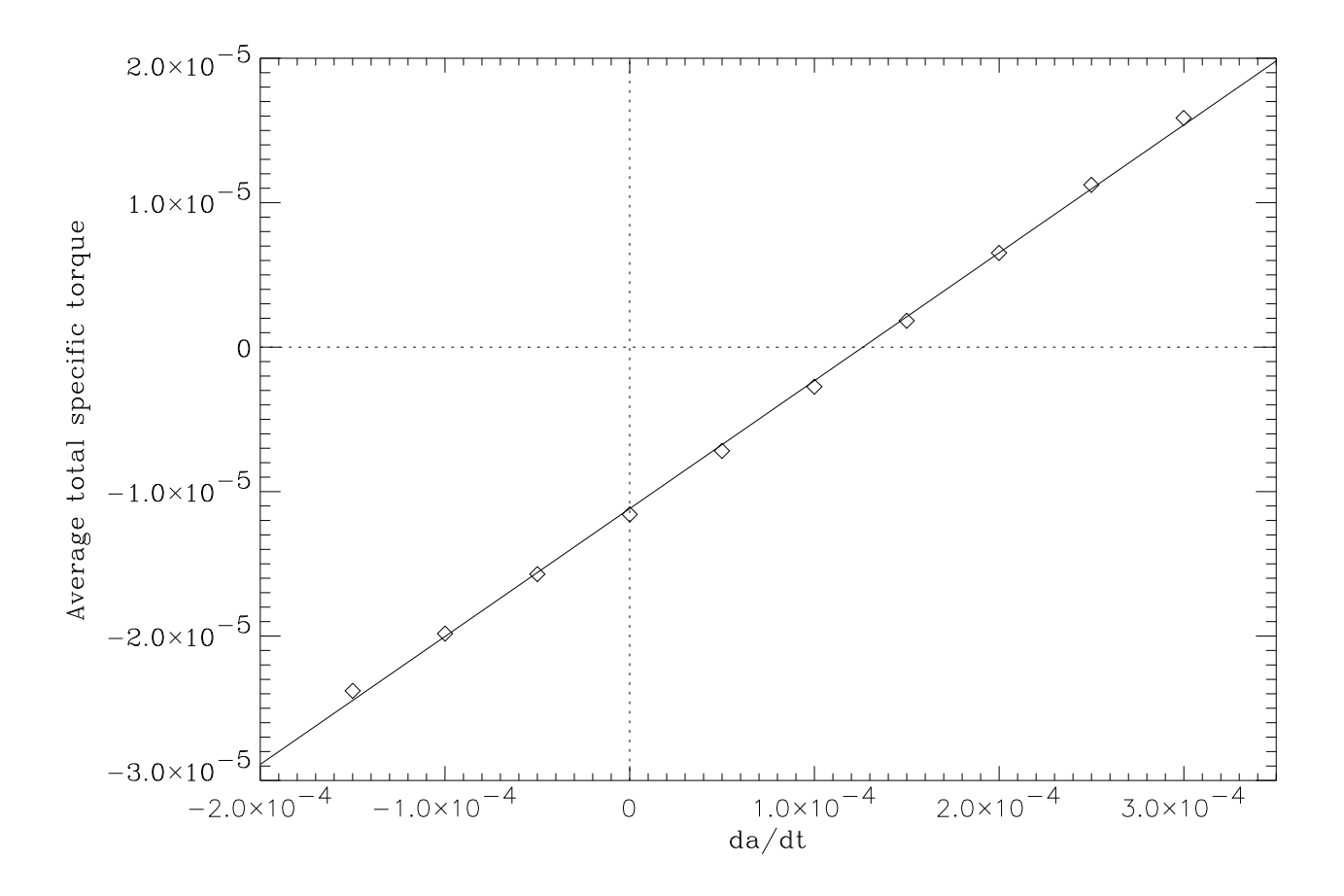


Fig. 8.— Average total specific torque value over the time interval [100, 200] orbits for the runs of Fig. 7, as a function of the imposed drift rate. The solid line shows the linear regression fit performed on the runs. The torque value for da/dt = 0 corresponds to the differential Lindblad torque (one can notice that this value is much smaller than what is given by a linear estimate, mainly because of the strong perturbation of the surface density profile). Also note, as stated in § 5.2, that the resolution used in our runs is just barely sufficient to get a proper estimate of the Lindblad torques for the very thin disks that we consider, whereas it is largely enough to describe properly coorbital effects.

since  $\delta m$  scales with  $\Sigma$ , and since the runaway starts for  $\delta m = M_p$ . If we call  $\mathcal{S}$  the slope of  $\gamma_{\text{tot}}$  as a function of  $\dot{a}$ , then we have:

$$2B_p a \frac{\Sigma}{\Sigma_{\text{crit}}} = \mathcal{S}. \tag{33}$$

The linear regression fit displayed at Fig. 8 yields S = 0.088, from which one infers  $\Sigma_{\rm crit} = 5.7 \cdot 10^{-4}$ , in good agreement (within  $\sim 15$  %) with the estimate given by the linear regression fit of Fig. 4. This is however only in rough agreement with the result given by the coorbital mass deficit estimate.

These additional runs also enable one to check whether the assumption that the horse-shoe zone width does not depend upon the drift rate is valid or not. We evaluate the distance  $x_s$  of the inner separatrix to the orbit at time t=150 orbits for all the runs. We find that  $x_s=0.105\pm0.005$  and that this quantity exhibits no systematic trend with  $\dot{a}$ .

## 5.6. Corotation torque in the fast migration regime

The previous section illustrates the linear dependency of the coorbital corotation torque on the drift rate in the slow migration regime (i. e.  $\dot{a} \ll |A_p| x_s^2/\pi a$ ). In order to investigate the fast migration regime, and in particular in order to get an idea of the migration rates that can be achieved in a runaway episode, it is of interest to know the  $\Gamma(\dot{a})$  relationship for large values of  $\dot{a}$ . The problem in that regime is that if an external operator imposes a fixed large drift rate to the planet, this latter sweeps a sizable fraction of its initial orbital radius in a very short time, and no reliable value can be measured for the corresponding torque. A workaround can be found as follows. As the torque that we aim at measuring arises from a relative drift of the disk material with respect to the planet horseshoe region, one can mimic this drift by adding an external specific torque to the disk material in order to make the fluid elements drift radially, while the planet is held on a fixed circular orbit. That way a steady state situation can be achieved, which allows a precise measurement of the torque even for very large drift rates. Namely, we performed a number of runs for which:

- 1. the planet is held on a fixed circular orbit with radius a=1,
- 2. the disk material undergoes an additional, external specific torque, with expression:

$$\gamma_{\text{add}} = \frac{2B(r)av_d \Sigma_p}{\Sigma_0(r)},\tag{34}$$

where  $v_d$  is the disk material radial drift velocity at the planet orbit and  $\Sigma_0(r)$  the unperturbed surface density; this expression ensures that the radial drift velocity in an

axisymmetric situation, that is  $u = v_d \frac{\Sigma_p a}{\Sigma_0(r)r}$ , corresponds to a steady state situation (i. e. that  $\partial [\Sigma r u]/\partial r = 0$ ),

3. a source of disk material with the adequate surface density is set at the grid outer / inner boundary for  $v_d < 0 / v_d > 0$ . This ensures that no disk depletion occurs at large  $v_d$ , which would modify the surface density profile and therefore would affect the torque value.

This torque prescription leads to the radial drift of any structure in the surface density profile in much the same way as for a viscous drift, but contrary to this latter it does not lead to a radial spread of the profiles. We ran 16 such configurations, with  $v_d^i = -5 \cdot 10^5 \times 2^{i/2}$  $(0 \le i \le 15)$ . As this corresponds to an inwards drift of the disk material, the upstream separatrix is the outer separatrix, and therefore the torque value should correspond to the ones measured at the previous section for positive values  $\dot{a}$ . The results are presented at Figs. 9 and 10. Clearly there is a satisfactory agreement between these results and the results obtained at the previous section for the case of true slow migration, as can be seen on the left part of the plots. This validates this method as an alternate way of measuring the corotation torque dependence on the migration rate. This agreement can be understood using similar arguments as the ones used by Masset (2001) to evaluate the corotation torque in a viscous disk. The librating fluid elements define a trapped region, the angular momentum of which is therefore constant in time. The external torque applied on this region is therefore exactly transmitted to the planet in a steady state situation. One can easily show that to lowest order in x/a an expression similar to Eq. (20) is obtained for the corotation torque. The agreement between the measured torques for a drifting planet and for a backward drifting disk, as well as the similarity of the flow topology in the  $(\theta, r - a)$  plane in either case, suggests that the torque measurement for a drifting disk, even in the fast migration limit, gives a reasonable idea of the behavior of the corotation torque on a migrating planet. This new method also offers the advantage that the planet is fixed with respect to the grid, and therefore there is no torque modulation as observed in Fig. 7 when the planet sweeps the mesh zones, and thus it enables us to get a more precise estimate of the disk torque. The critical drift rate for fast migration is:

$$|\dot{a}_c| = \frac{|A_p|x_s^2}{2\pi a}. (35)$$

Below this rate, all of the disk fluid elements crossing the upstream separatrix undergo a horseshoe like close encounter with the planet, and contribute to the corotation torque, while above this rate, some of them miss the planet. In the fast regime, which corresponds to the right part of the plots of Figs. 9 and 10, the corotation torque reaches a maximum value and

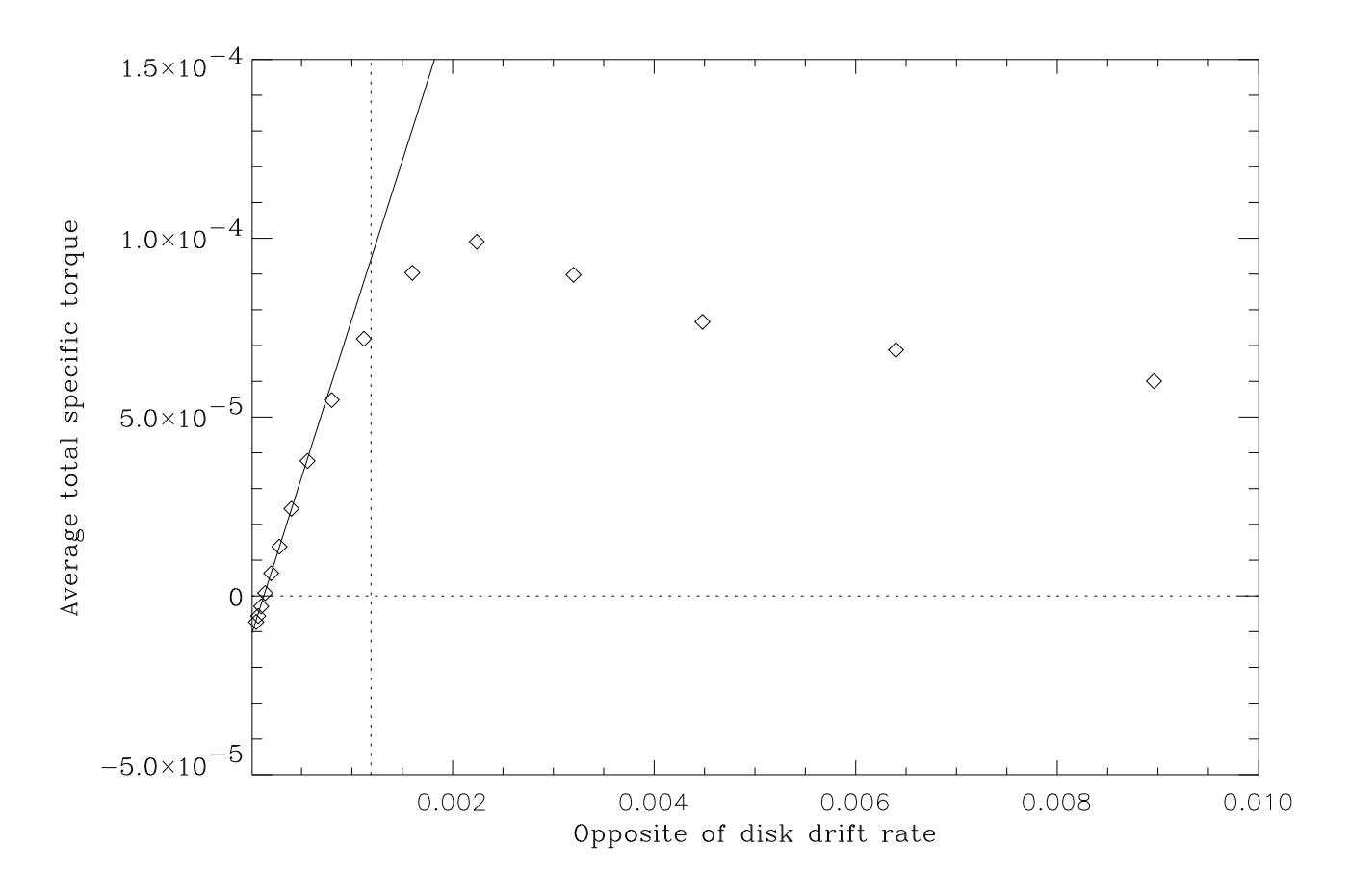


Fig. 9.— Total specific torque acting on the planet as a function of the opposite of the imposed disk drift, with a linear scale on the x-axis. The solid line shows the linear regression fit that was obtained from the data of Fig. 8. The vertical dotted line shows the critical drift rate  $|\dot{a}_c|$  for fast migration.

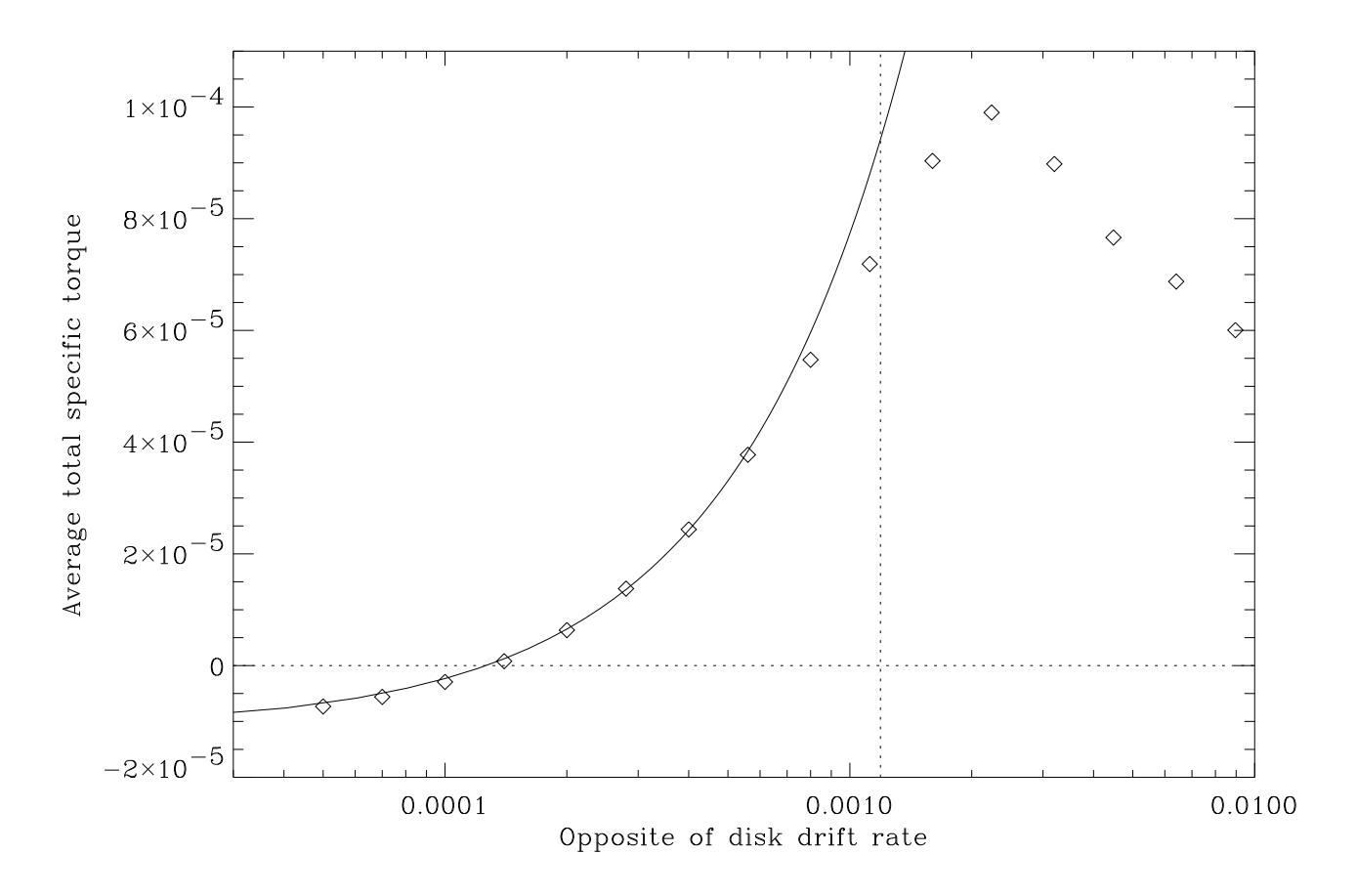


Fig. 10.— Same as Fig. 9 with a logarithmic scale on the x-axis. This plot offers a number of similarities with the torque versus viscosity relationship (Masset 2002).

then slowly decays, while its characteristic order of magnitude is:

$$\Gamma_{\text{fast}} = 2B_p a \,\delta m \,\dot{a}_c. \tag{36}$$

In the series of runs presented in section 5.4,  $\delta m$  scales with the disk surface density. The maximum drift rate should therefore roughly scale with the disk surface density during a runaway episode. This is in agreement with the results displayed at Fig. 3.

## 5.7. Outward runaway migration

Since in the runaway regime the differential equation governing the time evolution of the planet semi-major axis is second order in time, it is formally possible to have an outward migration for an adequate choice of the initial a and  $\dot{a}$ . For an outward migration, the upstream separatrix is the outer one. The higher the (inverse of) specific vorticity jump across that separatrix, the easier it is to get an outward migration. Therefore, outwards migration should be easier to get for shallower surface density profiles (corresponding to steeply increasing profiles of  $\Sigma/B$ ). The weakening of the differential Lindblad torque for shallower surface density profiles (Tanaka et al. 2002) plays in the same direction, since this torque tends to favor inward runaway rather than outward runaway. In order to illustrate this trend, we have performed a series of runs in which we hold the planet on a fixed  $\dot{a} > 0$ orbit for 100 orbital times, and then release it (i. e. we allow it to freely migrate under the action of the disk torque). The planet mass, disk aspect ratio and viscosity, the grid resolution and the numerical algorithm were strictly the same as in section 5.4, the disk surface density was  $\Sigma(r) = 10^{-3} r^{\alpha}$ , corresponding for r = 1 to  $\mathcal{S} = 10$ , i. e. approximately 50 % above the runaway critical surface density. We tried four values for  $\alpha$ : -3/2, -1, -1/2, and 0, corresponding to an increasingly shallower surface density profile. The starting semimajor axis is a = 0.7, and the semi-major axis at the time of release (t = 100 orbital times)is a=1, which ensures that in the four runs the disk surface density at the planet orbit is the same at the release time, and only differs by its slope. We see in Fig. 11 that the planet undergoes an inward runaway for the two steepest surface density profiles, and an outwards runaway for the two shallowest. The maximum  $\dot{a}$  is of the same order of magnitude in the four cases, and the runaway starting time, corresponding to the short exponential regime in which migration can be considered as slow ( $|\dot{a}| < |\dot{a}_c|$ ), is of the order of ten orbits, comparable to the outermost horseshoe libration time. This illustrates that a common mechanism is at work for the inward and outward runaways, and that these are tightly linked to the coorbital dynamics.

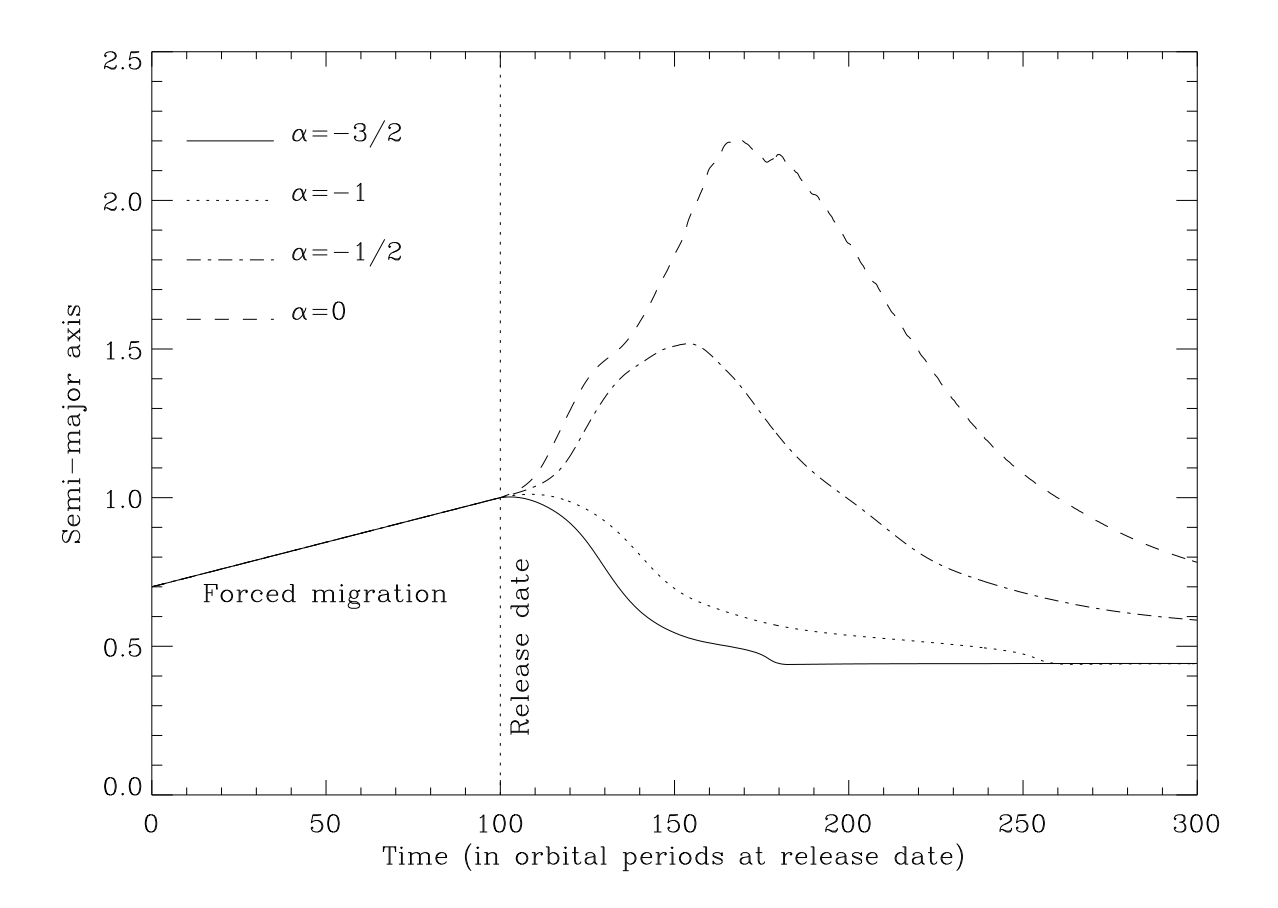


Fig. 11.— Time evolution of the planet semi-major axis for the four runs detailed in text. An outward runaway occurs for the two shallowest surface density profiles. The inner grid boundary is located at r = 0.4, and the curves lose significance whenever the planet get close to this inner boundary.

#### 6. Discussion

## 6.1. Occurrence of runaway migration

In order to assess the importance of runaway migration in protoplanetary nebulae, we have tried to delineate the runaway migration domain borders in a (planet mass, disk mass) space, while keeping the disk aspect ratio and viscosity fixed. All our disks have  $\Sigma_0(r) \propto r^{-3/2}$ , and a viscosity  $\nu = 10^{-5}$ . We tried three values of the disk aspect ratio: h = 0.03, 0.04 and 0.05, corresponding respectively to values for the  $\alpha$  parameter  $1.1 \cdot 10^{-2}$ ,  $6.3 \cdot 10^{-3}$  and  $4 \cdot 10^{-3}$ . We call disk mass the quantity  $m_D = \pi a^2 \Sigma_0(a)$ , and disk reduced mass the quantity  $\mu = m_D/M_*$ . The critical disk mass for runaway depends on the planet mass, as it depends on the dip shape around the orbit and on the position of the separatrices. In order to determine the disk critical mass, we measure the disk torque exerted on the planet, which is held on a fixed circular orbit, for the case where we exert no additional torque on the disk material (we do not impose any additional disk radial drift other than the one arising from its viscous evolution), and for the case where we exert an additional torque on the disk material (which corresponds to imposing an additional radial drift of the disk material with velocity  $v_d$ ). In the first case we measure a torque  $\Gamma$ , and in the second case a torque  $\Gamma'$ . From Eq. (22) and section 5.6, these two torques can be written respectively as:

$$\Gamma = \Delta \Gamma_{LR}$$

$$\Gamma' = \Delta \Gamma_{LR} - 2B_p a v_d \delta m, \qquad (37)$$

where  $\Delta\Gamma_{LR}$ , the differential Lindblad torque, is assumed to be independent of the disk radial drift velocity, and where the "static" part of the corotation torque vanishes since we consider initially a uniform specific vorticity disk. As the planet is held on a fixed circular orbit and a stationary state is reached, one can use Eq. (32), which yields:

$$\Sigma_{\text{crit}} = -\frac{2B_p M_p v_d \Sigma}{\Gamma' - \Gamma} = -\frac{2B_p v_d \Sigma}{\gamma' - \gamma},\tag{38}$$

where  $\gamma = \Gamma/M_p$  and  $\gamma' = \Gamma'/M_p$ . The value  $v_d$  must be chosen small enough so that it corresponds to the slow migration limit, and large enough that it allows an accurate measurement of  $\gamma' - \gamma$ . Preliminary runs have shown that an accurate estimate of the critical surface density can be reached with a value of  $v_d$  as small as  $2 \cdot 10^{-5}$ , corresponding to a disk radial drift which amounts to less than one zone radial width over the whole simulation, which illustrates the fact that even a small resolution grid, with a reduced number of zones across the horseshoe region, captures remarkably well most of the features of the corotation torque, as noted by Masset (2002). The measurement of  $\gamma$  and  $\gamma'$  can be performed in two different ways:

- either we perform two different runs with constant values of the disk drift, 0 and  $v_d$  (method 1),
- or we perform one run with a vanishing additional disk drift, and once a steady state is reached we switch the drift to  $v_d$ . The new torque value can then be measured after a horseshoe libration time (method 2).

The first method is better suited to small mass planets, for which the libration time is prohibitively long, while the second method is well suited for higher mass planets, since it allows almost a 50 % saving of CPU time compared to the first method. For intermediate, Saturn mass planets we used both methods to check that they give comparable results. The results are presented at Figs. 12, 13 and 14. These plots lead to a number of comments:

- The thinner the disk, the larger the runaway domain. This corresponds to expectations: for a given planet mass and disk viscosity (such that the planet mass is smaller than the viscous gap opening criterion), the thinner the disk, the deeper the dip opened around the orbit, and therefore the larger the coorbital mass deficit.
- In the three cases, the mass most favorable to runaway (corresponding to the minimum of the critical disk mass curve) is  $\sim 0.3 0.4 M_J$ , or typically a Saturn mass.
- Runaway migration can be found in relatively massive protoplanetary disks (a few times more massive than the minimum mass solar nebula, depending on the protogiant semi-major axis).
- Runaway migration should be common, in such disks, for giant protoplanets which reach a sizable fraction of a Saturn mass.
- The right part of the domain boundary shows a steep rise around 1  $M_J$  in the three cases.
- Even in a disk with  $\Sigma \propto r^{-3/2}$  such as the MMSN, runaway migration is more difficult as one gets close to the star. The coorbital mass deficit scales indeed as  $a^2\Sigma(a) \propto \sqrt{a}$ .
- The analysis performed breaks down for lower mass planets  $(R_H < H)$ , as the torque cannot reliably be estimated through a 2D calculation. The runaway limit for the low mass planets at the left of the vertical dashed line is likely higher than found in our analysis, as in their case only a fraction of the disk vertical extent is involved in the coorbital dynamics.

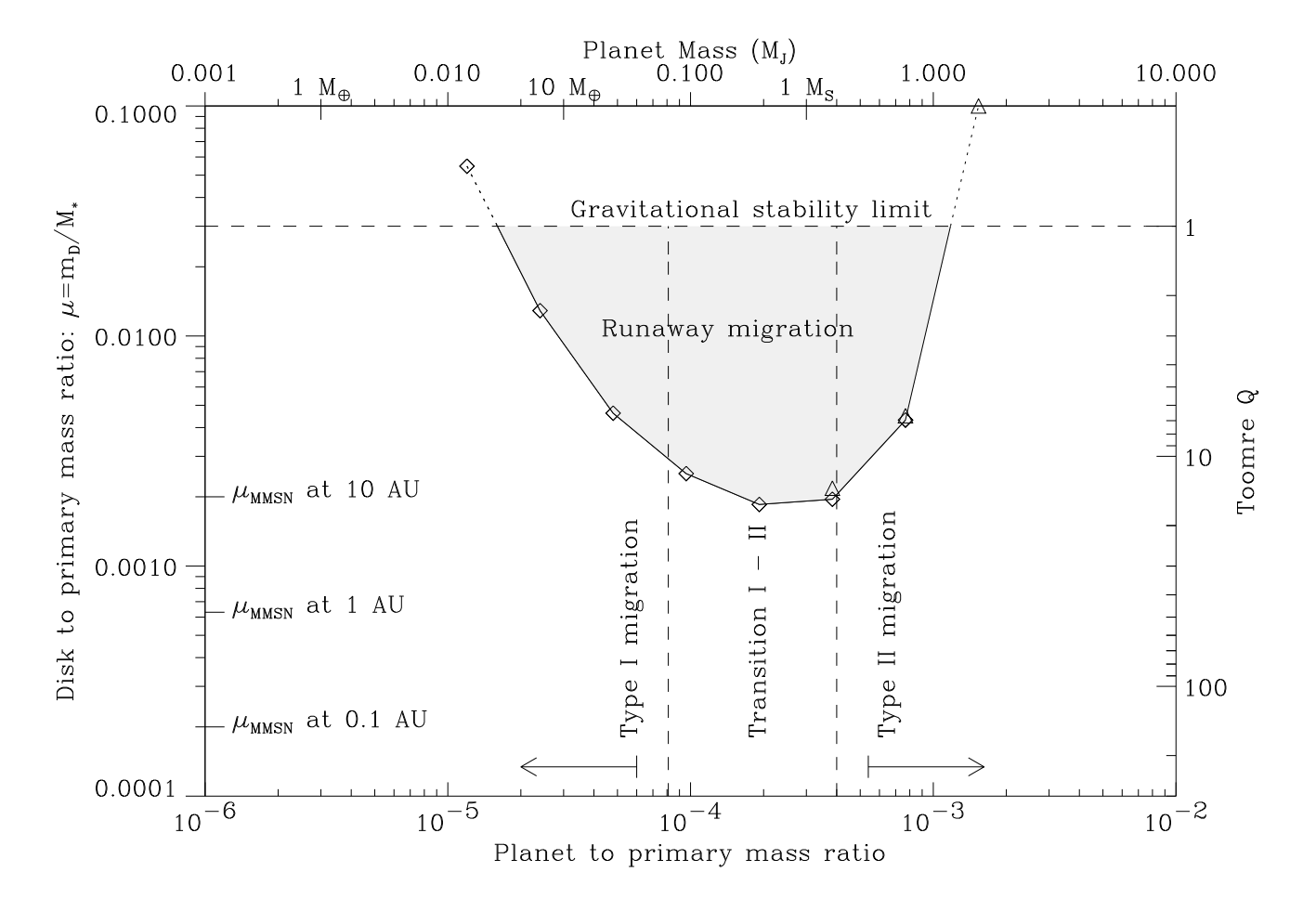


Fig. 12.— Runaway migration domain for a 3 % aspect ratio disk with viscosity  $\nu=10^{-5}$ . The domain horizontal upper limit corresponds to the Q=1 gravitational stability limit (which translates into  $\mu=h$ ). The left vertical dashed line shows the limit of linear type I migration, and corresponds to  $R_H=H$ , where  $R_H$  is the planet Hill radius. Note that Miyoshi et al. (1999) find a threshold for non-linear effects for even lower masses ( $R_H=H/2$ ), which corresponds to a factor 8 in the mass. The right vertical dashed line corresponds to the viscous gap opening criterion  $q>40/\mathcal{R}$ , where  $\mathcal{R}=a^2\Omega(a)/\nu$  is the disk Reynolds number at the planet orbit (Papaloizou & Lin 1984), beyond which the disk is split into an outer and an inner disk, and the planet is locked in the disk viscous drift (type II migration). Diamonds indicate the critical values found using method 1 (see text), while triangles indicate critical values found using method 2. The tick marks on the left axis represent the reduced disk mass of the minimum mass solar nebula respectively at 10, 1 and 0.1 AU. The upper axis shows the planet mass in Jupiter masses if one assumes that the central object has one solar mass.

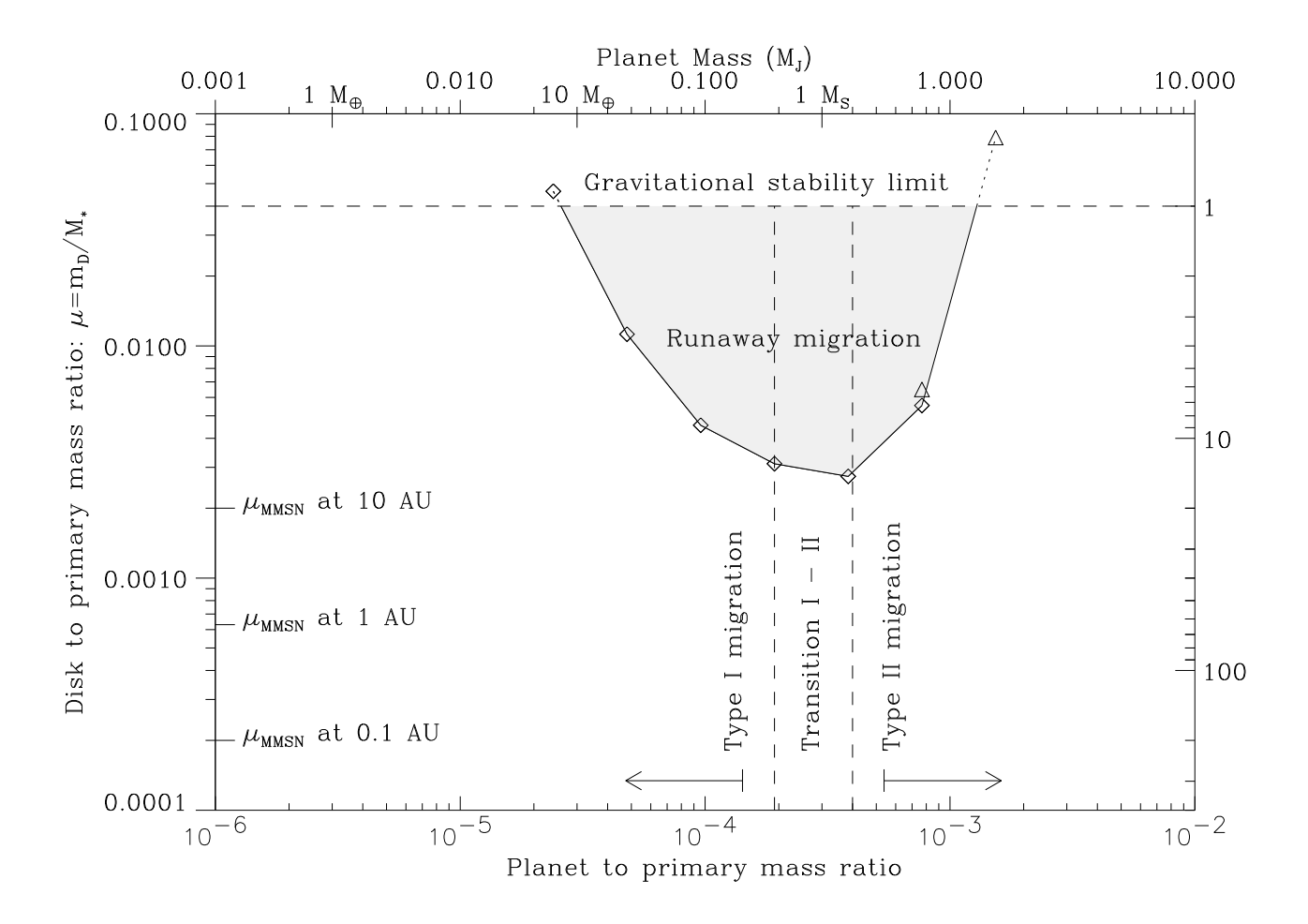


Fig. 13.— Same as Fig. 12 for a h=4 % aspect ratio disk.

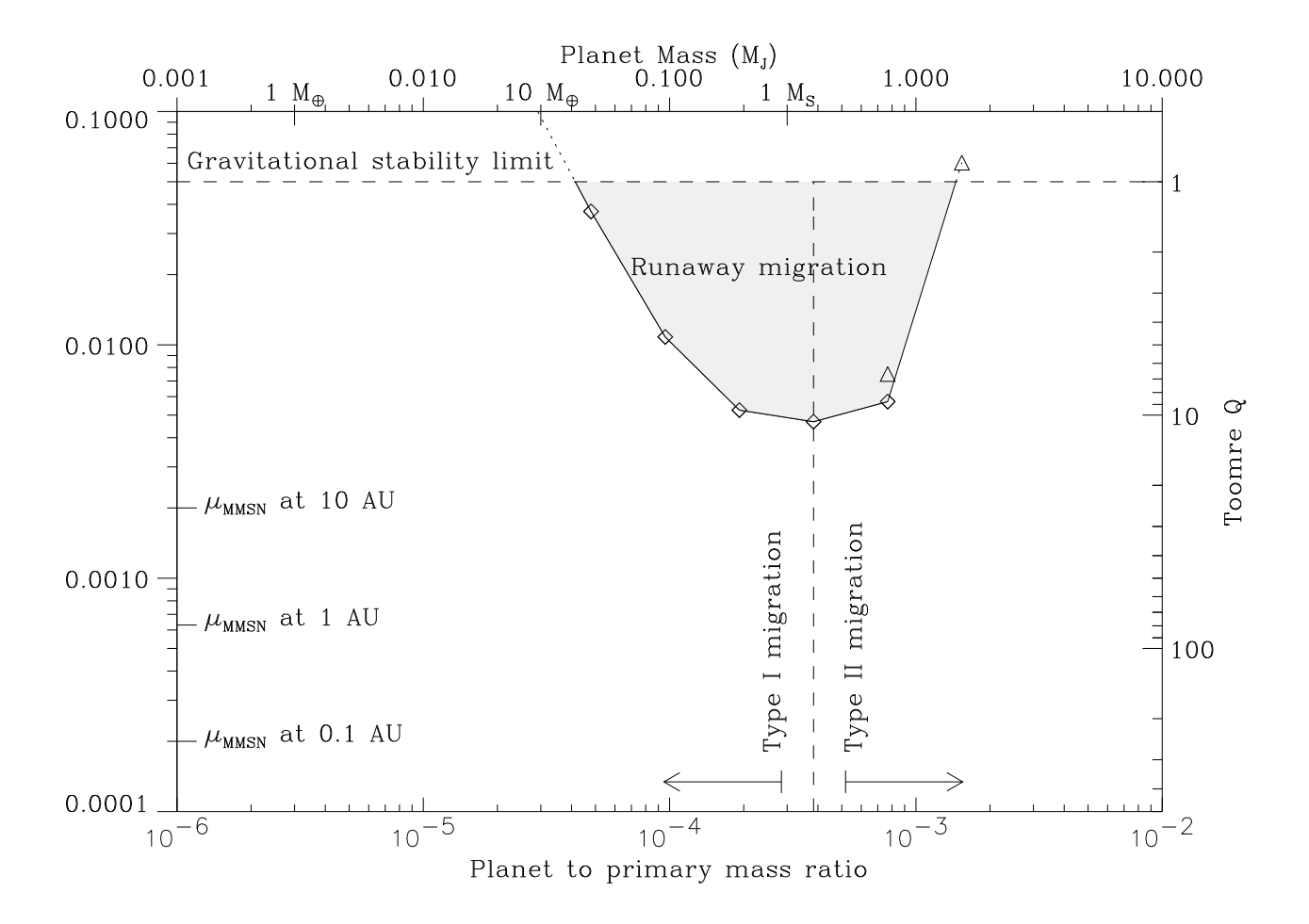


Fig. 14.— Same as Fig. 12 for a h=5~% aspect ratio disk

#### 6.2. Additional effects

The viscosity chosen for these runs is high enough that the dip viscous time  $\tau \sim w^2/3\nu$  is comparable to the libration time ( $w \simeq x_s$  being the dip half-width). This time is also the dip opening time when the planet is "switched on" in the disk, or also the minimum time that the planet needs to sweep radially its own dip radial width in order for the surface density profile depression to follow the planet migration. It is therefore possible to talk unambiguously of the disk runaway critical mass for a given planet, independently of its "preparation state". In other words, whether we release ab initio the planet in an unperturbed disk, or whether we hold it on a fixed circular orbit for a few hundreds of orbits in order to allow it to open a dip before being released makes no difference: a runaway is observed above the same disk mass, and the maximum drift rate measured is the same in both cases. If one tries to delineate the runaway domain for a disk with a much smaller viscosity, one finds that the estimate strongly depends on the disk "preparation state", contrary to the case of Figs. 12 to 14. One can achieve indeed a significant coorbital mass deficit if one holds the planet on a fixed circular orbit for a sufficient amount of time. Simulations performed for Saturn mass planets in massive, low viscosity disks display a very erratic behavior, with an alternation of brief runaway episodes followed by moderately eccentric ( $e \sim 0.01$ ), halted migration episodes, the overall drift rate being a relatively small but sizable ( $\sim 20 \%$ ) fraction of the corresponding type I drift rate.

It is of interest to evaluate the type I to runaway drift rate ratio at the critical disk mass  $\mu_c$  for runaway, as a function of planet mass. At this boundary, Eq. (36) leads to  $\dot{a} = \dot{a}_c$  (since  $\delta m = M_p$ ), whereas the type I drift rate in the same disk, according to Eq. (70) of Tanaka et al. (2002), is given by:

$$\dot{a}_I = 1.38\mu_c q h^{-2} \Omega_p a. \tag{39}$$

Fig. 15 shows the ratio of the runaway to type I migration rate estimate, as a function of planet mass, for the three aspect ratios presented in Figs. 12 to 14. These ratios are estimated at the critical disk mass for runaway. Since the maximum runaway drift rate scales roughly with the disk mass (see sect. 5.6), this ratio should not vary significantly if one considers disk masses higher than the critical one. One can see that this ratio is marginally larger than unity for slightly sub-Saturn mass planets, and drops considerably for smaller and larger masses. The runaway drift rate estimate is however still considerably larger than the type II viscous drift rate estimate for a Jupiter mass planet, as it corresponds typically to the third of the type I drift rate of a Saturn mass planet.

The main source of the effect we have presented is the drift across the separatrices of the coorbital region of inner / outer disk material, in the cases of inward / outward planet drift

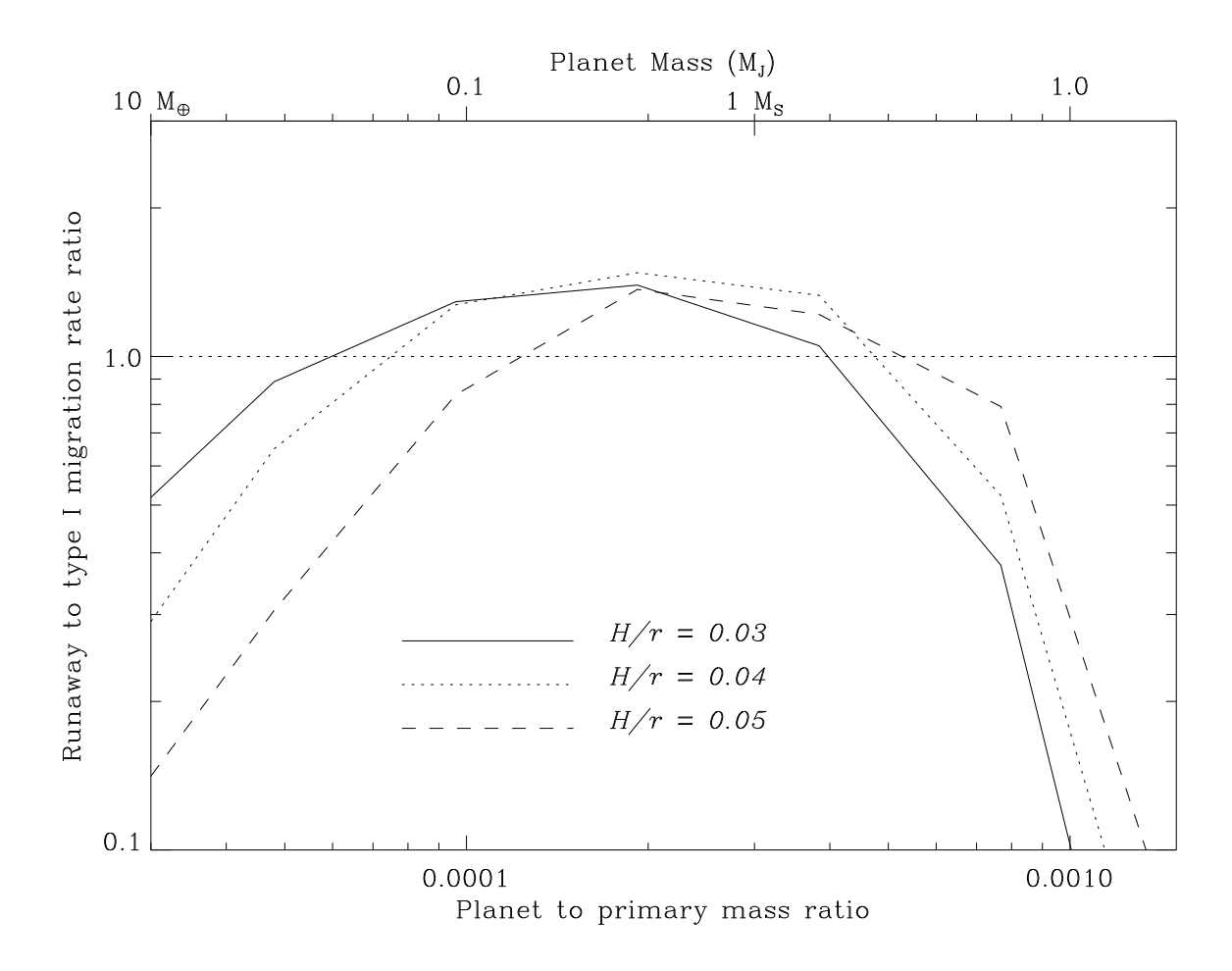


Fig. 15.— Ratio of runaway to type I drift rate, at the critical disk mass.

respectively. We have assumed that the drift velocity of the planet with respect to the disk is  $\dot{a}$ , thereby neglecting the disk viscous drift rate  $\sim -(3/2)\nu/r$ . Taking this additional drift into account would add a positive contribution to the corotation torque  $\sim 3B_p \, \delta m \, \nu$ . For the case of a weak coorbital depletion,  $\delta m \propto \Gamma_{\rm LR}/\nu$ , so that this additional term scales as  $\Gamma_{\rm LR}$ , the one-sided Lindblad torque. This additional term, coupled to the one-sided Lindblad torque, has been evaluated to order of magnitude by Masset (2001, 2002), and found to be small. Since furthermore it does not participate in the feed back and therefore in the runaway, it is legitimate to have neglected it in the present analysis.

The ability of the planet to maintain its coorbital mass deficit during a runaway episode deserves further investigation. Before runaway, the coorbital region is partially cleared of disk material under the action of the Lindblad torques. During the runaway drift, the Lindblad torques are assisted in maintaining the coorbital mass deficit by the horseshoe dynamics, which traps the coorbital material. The streamlines are not exactly closed in the  $(\theta, r - a)$  space, however, and the coorbital material can be lost. In that case the coorbital region is no longer depleted, and the planet switches to type I migration, which endows it with a comparable drift rate. No case has been found in which the runaway is maintained "forever". A single runaway episode however can sizably affect the planet semi-major axis, by a factor 2 or more.

In this work we have neglected accretion onto the protoplanets, whereas the mass range for which the runaway mechanism is relevant seems to imply gas accretion. A runaway episode is likely to be accompanied by a simultaneous accretion of disk material. A simple way to take into account gas accretion is to consider that a fraction  $\varepsilon$  of the material which enters the coorbital zone through one separatrix and flows out along the other one, is kept by the planet. In the absence of accretion, this disk material contribution to the corotation torque amounts to  $\Gamma_2 = 4B_p ax_s \cdot 2\pi a\dot{a}\Sigma(x_s)$ . When accretion is considered, the contribution to the corotation torque reduces to:

$$\Gamma_2' = (1 - \varepsilon)\Gamma_2 + \frac{1}{2}\varepsilon\Gamma_2,\tag{40}$$

since the material that is accreted onto the planet loses/gains only half of the specific angular momentum that it would lose/gain otherwise. Accretion therefore plays the role of a runaway moderator. It would be of interest to investigate in detail the interplay between runaway and accretion, taking consistently into account the corotation torque feed back reduction and the growth of the horseshoe region.

## 7. Summary and conclusions

We have evaluated the torque exerted on a protoplanet embedded in a gaseous disk produced by the fluid elements as they perform a horseshoe U-turn in the planet vicinity. We have interpreted this torque as the coorbital corotation torque. This torque exhibits a dependency upon the planet radial drift rate in the disk which is tied to the depletion of the coorbital region of the planet, that is to say to the existence of a dip or gap cleared around the orbit. The sign of the corotation torque is the same as that of the drift rate. Hence it exerts a positive feed back on the migration process. This feed back leads to a migration runaway in massive disks when the coorbital mass deficit is larger than the planet mass. We have checked and illustrated the main properties of the corotation torque through customized numerical simulations. These showed the link between runaway and the coorbital mass deficit. They indicated that the migration rate for disks with sub-critical masses grows faster than linearly with disk mass, and they illustrated that the planet drift rate characteristic response time is the horseshoe libration time.

The occurrence of inward runaway in disks with  $\Sigma \propto r^{-3/2}$  has been investigated, and found to be likely in thin  $(h \leq 5 \%)$ , massive disks with a mass several times that of the MMSN. Typically it occurs for Saturn-sized giant protoplanets, but it can involve planets up to one Jupiter mass for sufficiently massive disks. The runaway drift rate is found to be comparable to the type I estimate given by the differential Lindblad torque that one would obtain using linear theory even though that would be invalid for a planet held in a fixed circular orbit (because the planet opens a significant dip around its orbit and the actual differential torque acting on it amounts to a small fraction of its linear estimate). It turns out that the corotation torque is at most equal to the differential Lindblad torque in a  $\Sigma \propto r^{-3/2}$  disk. This prevents the possibility of outward runaway in these disks, and we indeed found no occurrence of outward runaways in such disks. Additional runs with shallower disk profiles however have shown that outward runaway can occur, provided the planet is endowed with an adequate value for a and  $\dot{a}$  (this latter needs to be established at least over a libration time).

The way we initiated outward runaway was artificial. Masset & Snellgrove (2001) have exhibited a two planet configuration engaged in an outward migration. Their outer planet is of Saturn mass, and is therefore a good candidate for outward runaway in a massive disk. An alternate possibility to initiate an outward motion is that the disk mass flow across the orbit is strongly variable in time. If a larger  $\dot{M}$  enters the coorbital zone through the outer separatrix, the corotation torque may be temporarily large (and positive), providing the seed for an outward runaway.

When the viscosity is large enough, that the viscous diffusion time across the horseshoe

zone is faster than the time to migrate through it, relaxation and depletion of the coorbital region occurs in a sufficiently short amount of time that the coorbital mass deficit and the disk critical mass for runaway are well defined quantities. The situation turns out to be much more chaotic in a very low viscosity disk, although globally the average drift rate of the planet towards the central object amounts to a sizable fraction of the type I drift rate.

Inspection of Figs. 12 to 14 shows that in massive disks, sub-Jovian planets can still undergo a type I like drift, whereas on previous grounds they were expected to have a much slower (type II) drift rate, comparable to the slow viscous disk drift rate.

The runaway threshold is lower in thinner disks. If protoplanetary disks are flared (i. e.  $\partial \log H/\partial \log r > 1$ ), they could be extremely thin in their inner regions, which could assist runaway there.

A runaway episode or a succession of them stops whenever the coorbital mass deficit that can be achieved is too small. If one assumes a disk surface density profile  $\Sigma(r) \propto r^{\alpha}$ , then the coorbital mass deficit scales as  $\delta m \propto a^2 \Sigma(a) \propto a^{2+\alpha}$ . As the runaway condition reads  $M_p = \delta m$ , one would get, at the end of the runaway episodes, the relationship  $M_p \propto P^{(4+2\alpha)/3}$ , where P is the planet orbital period. This indicates a tendency for smaller masses to reach smaller periods. A recent analysis by Zucker & Mazeh (2002) indicates a paucity of planets with masses exceeding a Jupiter mass at small periods  $\sim$  a few days while sub Jovian mass planets tend to cluster at these small periods. The observational data for the larger mass planets is consistent with a type II migration scenario in which most time is spent at larger radii (Trilling et al. 2002). However, the distribution of smaller mass objects would appear to require a relatively fast migration of the type discussed here followed by a slowing down or stopping near their current orbital locations. The fate of a giant protocore at the end of its runaway episode(s) if it has not been brought close to the primary, would be a slow, type II migration, together with a possible mass growth, along the lines already studied e. g. by Nelson et al. (2000) followed possibly by stopping inside a magnetospheric cavity.

An alternative scenario could be envisaged to account for the properties of EGPs. In this, the disks in which they formed would have been massive enough to sustain a succession of runaway episodes typically up to the central tenth of an astronomical unit where hot "Jupiters" with  $M \sin i \sim 0.3~M_J$ , roughly corresponding to the most favorable mass for runaway, are found to accumulate (or alternatively protocores that massive could be constituted in situ by the accumulation of lower mass bodies brought there by type I migration.) Some of these hot proto-Saturns could then be involved in outward runaway. At the same time, gas accretion onto these cores would eventually endow them with a mass sufficient to prevent any further runaway migration episodes. These planets would then correspond to the massive  $(M_p > 1 - 2~M_J)$  extrasolar planets, which are found further out from their host

stars than the hot Jupiters.

Computational resources were available at the CGCV Grenoble, and are gratefully acknowledged.

# A. Corotation torque on a migrating planet for a given specific vorticity profile

We transform Eq. (11) using the fact that a coorbital fluid element does not undergo any radial drift (we assume a low viscosity) between two successive close encounters and we write:

$$w_L^-(x,t) = w_R^-[x + a(t) - a(t-\tau), t-\tau],\tag{A1}$$

where we use the fact that the distance  $r = x + a(t - \tau)$  of the fluid element to the central object, just after the R-close encounter at time  $t - \tau$ , is the same as the distance r = x + a(t), just before the L-close encounter at time t. We now assume that the profile  $w_R(x,t)$  is independent of t for any x in  $[-x_s, +x_s]$ , which corresponds to assuming that either migration is steady state, or that it is slow enough that the surface density profile responds much faster than  $|x_s/\dot{a}|$ . We can therefore write:

$$w_{L}^{-}(x,t) = w_{R}^{-}(x,t) + [a(t) - a(t-\tau)] \frac{\partial w_{R}^{-}}{\partial x} + \frac{1}{2} [a(t) - a(t-\tau)]^{2} \frac{\partial^{2} w_{R}^{-}}{\partial x^{2}}.$$
(A2)

A Taylor expansion in  $\tau$  of this expression yields:

$$w_L^-(x,t) = w_R^-(x,t) + \tau \dot{a} \left( \frac{\partial w_R^-}{\partial x} + \frac{1}{2} \tau \dot{a} \frac{\partial^2 w_R^-}{\partial x^2} \right) - \frac{1}{2} \tau^2 \ddot{a} \frac{\partial w_R^-}{\partial x}. \tag{A3}$$

The second term of the bracket, an upper limit of which is  $\sim (1/2)\dot{a}\tau(\partial w_R^-/\partial x)/H$ , is negligible compared to the first one, as long as the migration remains slow. Eqs. (11) and (A3) yield:

$$\Gamma = 16\pi B_p^2 a^2 \left\{ \dot{a} \left( x_s w_R^-(-x_s) - \int_{-x_s}^0 w_R^-(x) dx \right) + \frac{\pi a \ddot{a}}{2|A_p|} [w_R^-(0) - w_R^-(-x_s)] \right\}.$$
(A4)

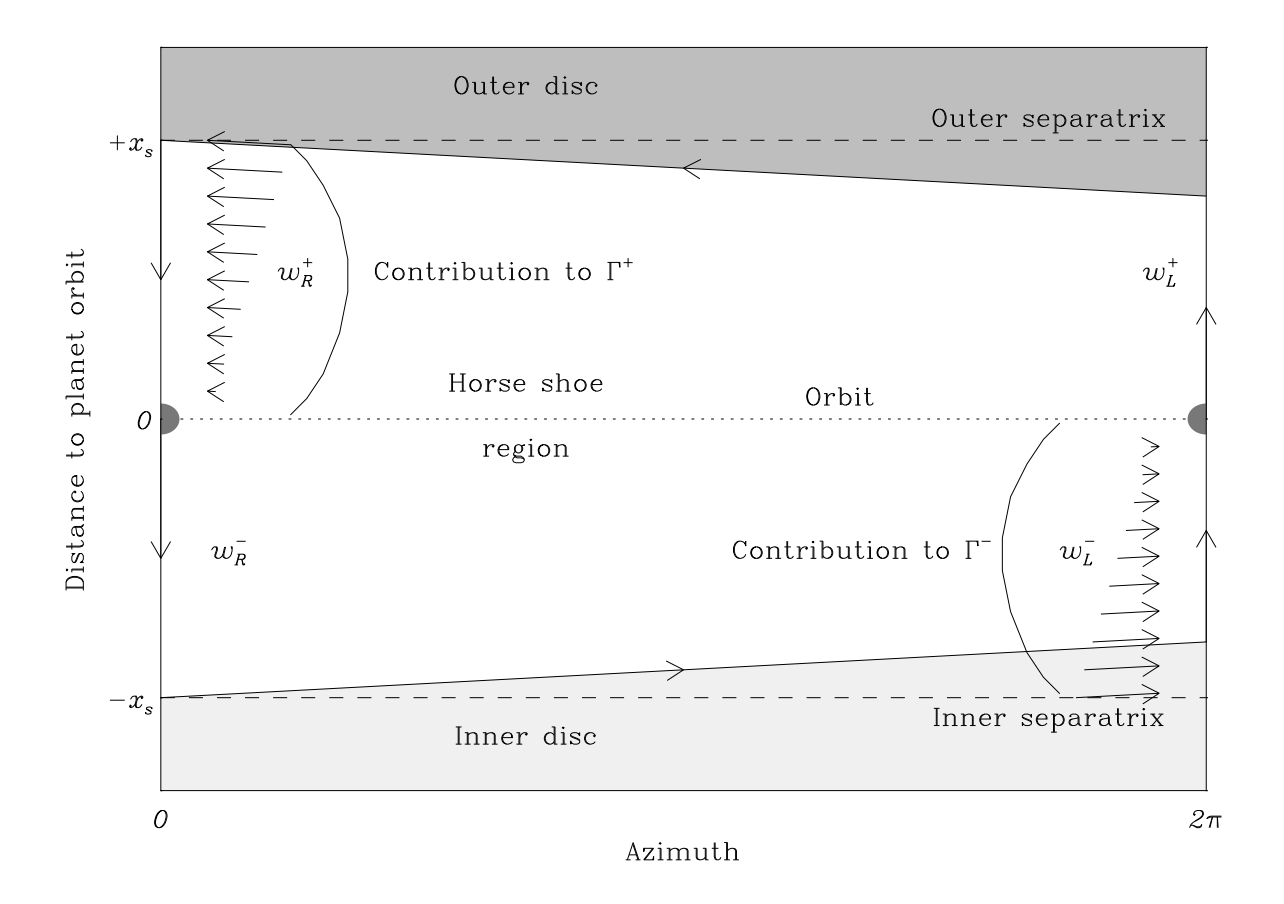


Fig. 16.— Sketch of the flow for the case  $\dot{a} < 0$ . We see that over the whole interval  $[-x_s, +x_s]$ , one has  $w_R(x) = w_R(-x)$ . On the other hand, one cannot write  $w_L(-x) = w_L(x)$  for any x in  $[-x_s, +x_s]$ , since fluid elements from the inner disk (light shaded region) contribute to the negative part of the corotation torque  $(\Gamma^-)$ , and therefore bring into the coorbital region new material, with a priori an arbitrary specific vorticity. The consequence of this distinction is that one has to evaluate the coorbital mass deficit from the upstream side of the coorbital depletion (i. e. in this case from the mass flow across the inner separatrix.)

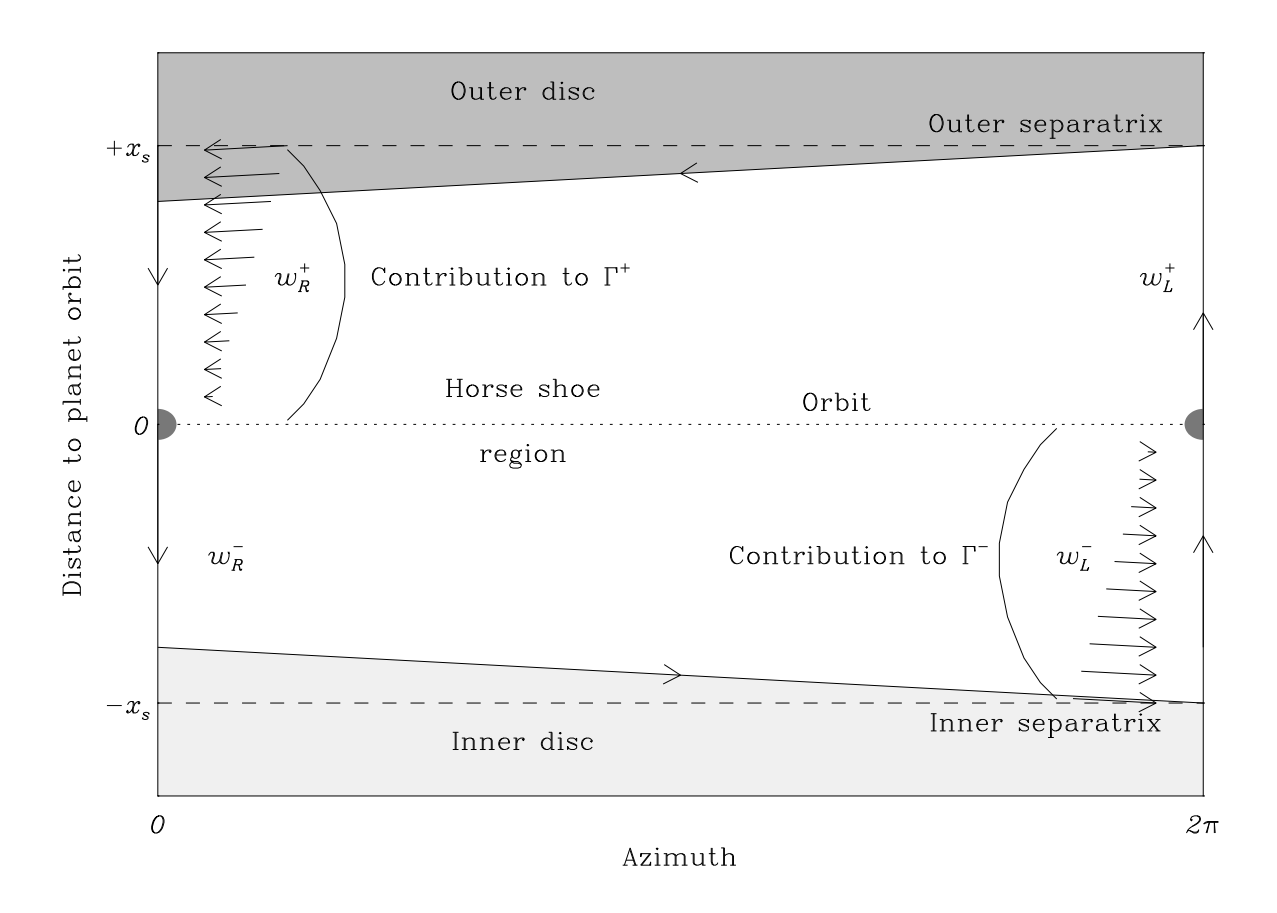


Fig. 17.— Same as Fig. 16 but with  $\dot{a} > 0$ . We see that over the whole interval  $[-x_s, +x_s]$ , one has  $w_L(x) = w_L(-x)$ . On the other hand, one cannot write  $w_R(x) = w_R(-x)$  for any x in  $[-x_s, +x_s]$ , as new material from the outer disk is involved in the corotation torque (heavy shaded region), and has a priori an arbitrary specific vorticity.

An order of magnitude estimate of the last term (in  $\ddot{a}$ ) of Eq. (A4) can be given if one assumes e. g. a quadratic dependency of  $w_R(x)$  on x:  $w_R(x) \propto x^2$ , in which case one has:  $w_R(-x_s) - w_R(0) = 3 \, \delta m / (16 \pi a x_s B_p)$ . Eq. (A4) can then be rewritten as:

$$\Gamma = 2B_p a \,\delta m \,\dot{a} - \frac{3\pi a^2 B_p}{2|A_p|x_s} \,\delta m \,\ddot{a},\tag{A5}$$

which is similar to Eq. (22), except for a factor 3/2 in the  $\ddot{a}$  term, which we had claimed to be given in order of magnitude only.

#### REFERENCES

Balmforth, N. J., Korycansky, D. G. 2001, MNRAS, 326, 833

Foglizzo, T. & Ruffert, M. 1997, A&A, 320, 342

Ivanov, P. B., Papaloizou, J. C. B. & Polnarev, A. G. 1999, MNRAS, 307, 79

Kley, W. 1998, A&A, 338, 37

Lin, D. N. C. & Papaloizou, J. C. B. 1986, ApJ, 309, 846

Masset, F. S. 2002, A&A, 387, 605

——. 2001, ApJ, 558, 453

Masset, F. & Snellgrove, M. 2001, MNRAS, 320, L55

Masset, F. S. 2000a, A&AS, 141, 165

———. 2000b, in Disks, Planetesimals and Planets, ASP Conference Series, Vol. 219, 75–80

Miyoshi, K., Takeuchi, T., Tanaka, H. & Ida, S. 1999, ApJ, 516, 451

Nelson, R. P., Papaloizou, J. C. B., Masset, F. S., & Kley, W. 2000, MNRAS, 318, 18

Papaloizou, J. C. B. & Terquem, C. 1999, ApJ, 521, 823

Papaloizou, J. C. B. & Lin, D. N. C. 1984, ApJ, 285, 818

Tanaka, H., Takeuchi, T. & Ward, W. R. 2002, ApJ, 565, 1257

Trilling, D. E., Benz, W., Guillot, T., Lunine, J. I., Hubbard, W. B. & Burrows, A. 1998, ApJ, 500, 428 Trilling, D. E., Lunine, J. I. & Benz, W. 2002, astroph/0208184

Ward, W. R. 1997, Icarus, 126, 261

——. 1992, Abstracts of the Lunar and Planetary Science Conference, 23, 1491

——. 1991, Abstracts of the Lunar and Planetary Science Conference, 22, 1463

Ward, W. R. & Hourigan, K. 1989, ApJ, 347, 490

Zucker, S. & Mazeh, T. 2002, ApJ, 568, L113

This preprint was prepared with the AAS IATEX macros v5.0.